Published in final edited form as:

Toxicol Pathol. 2021 July ; 49(5): 1077–1099. doi:10.1177/01926233211004433.

Role for mucin-5AC in upper and lower airway pathogenesis in mice

Hye-Youn Cho[1], **Soojung Park**[2], **Laura Miller**[1], **Huei-Chen Lee**[2], **Robert Langenbach**[2], **Steven R. Kleeberger**[1]

[1]Immunity, Inflammation and Disease Laboratory, National Institute of Environmental Health Sciences, National Institutes of Health, Research Triangle Park, NC

[2]Signal Transduction Laboratory, National Institute of Environmental Health Sciences, National Institutes of Health, Research Triangle Park, NC

Abstract

Mucin-5AC (MUC5AC) is a major secreted mucin in pathogenic airways. To determine its role in mucus-related airway disorders, *Muc5ac*-deficient (*Muc5ac*$^{-/-}$) and wild-type (*Muc5ac*$^{+/+}$) mice were compared in bleomycin-induced pulmonary fibrosis, respiratory syncytial virus (RSV) disease, and ozone toxicity. Significantly greater inflammation and fibrosis by bleomycin were developed in *Muc5ac*$^{-/-}$ lungs compared to *Muc5ac*$^{+/+}$ lungs. More severe mucous cell metaplasia in fibrotic *Muc5ac*$^{-/-}$ lungs coincided with bronchial *Muc2, Muc4*, and *Muc5b* overexpression. Airway RSV replication was higher in *Muc5ac*$^{-/-}$ than in *Muc5ac*$^{+/+}$ during early infection. RSV-caused pulmonary epithelial death, bronchial smooth muscle thickening, and syncytia formation were more severe in *Muc5ac*$^{-/-}$ compared to *Muc5ac*$^{+/+}$. Nasal septal damage and subepithelial mucoserous glands enrichment by RSV were greater in *Muc5ac*$^{-/-}$ than in *Muc5ac*$^{+/+}$. Ozone exposure developed more severe nasal airway injury accompanying submucosal gland hyperplasia and pulmonary proliferation in *Muc5ac*$^{-/-}$ than in *Muc5ac*$^{+/+}$. Ozone caused PAS-positive secretion only in *Muc5ac*$^{-/-}$ nasal airways. Lung E-cadherin level was relatively lower in *Muc5ac*$^{-/-}$ than in *Muc5ac*$^{+/+}$ basally and after bleomycin, RSV, and ozone exposure. Results indicate that MUC5AC is an essential mucosal component in acute phase airway injury protection. Subepithelial gland hyperplasia and adaptive increase of other epithelial mucins may compensate airway defense in *Muc5ac*$^{-/-}$ mice.

Keywords

MUC5AC; fibrosis; respiratory syncytial virus; ozone; nasal airway; lung; mouse

Correspondence should be addressed to: Hye-Youn Cho, Ph.D., Immunity, Inflammation and Disease Laboratory, National Institute of Environmental Health Sciences, Building 101, MD D-201, 111 TW Alexander Dr., Research Triangle Park, North Carolina 27709, Phone Number: 984-287-4088, FAX Number: 301-480-3977, cho2@niehs.nih.gov.

DECLARATION OF CONFLICTING INTERESTS STATEMENT

The author(s) declared no potential, real, or perceived conflicts of interest with respect to the research, authorship, and/or publication of this article.

INTRODUCTION

Mucus forms a hydrophilic gel layer over mucosal tissue surface in respiratory, gastrointestinal, and urogenital tracts as well as in visual and auditory systems to provide non-specific physical and biological barriers for innate defense. The respiratory track from nasal passages to conducting airways are lined by a complex epithelium containing mucus-producing surface mucous (goblet) cells. In addition, numerous submucosal glands in cartilaginous airways are either mucous (viscous, mostly mucus) or serous (watery, mostly with Cl^- and HCO_3^-) glands are composed of mucous cells [1]. Club cells (formerly Clara cells) in small airways also known to produce and steadily secrete low amounts of mucin [2,3]. The increased abundance of goblet (mucous) cells (metaplasia or hyperplasia) is a common response to inflammation following exposure to microbial pathogens, particles, and toxicants, resulting in increased mucus production and secretion [4]. In addition, submucosal gland secretions have synergistic effects with surface secretion in airway defense against pathological insults [5]. However, overproduction and hypersecretion of mucus often obstructs airways and contribute to pathogenesis of chronic obstructive pulmonary disease (COPD), asthma, and bronchiectasis and is associated with recurrent infection and morbidity or mortality [6,7].

Mucin is the core glycoprotein of mucus, and MUC5AC and MUC5B are among 22 defined mucin proteins (16 mucins in mice) discovered [8]. Two subfamilies of mucins are membrane-bound mucins (e.g., MUC1, MUC4) and secreted mucin glycoproteins (e.g., MUC2, MUC5AC/B); The secreted mucins are further subdivided into insoluble gel-forming (e.g., MUC2, MUC5AC/B) and soluble mucins [9,10]. Goblet cells in nasal respiratory epithelium to large bronchial epithelium constitutively synthesize, store, and secrete MUC5AC and MUC5B [2,3]. In contrast, submucosal gland acini in large airways primarily synthesize MUC5B [2,3], which is the most abundant secreted airway mucin in normal airways as the volume of the glands is about 50 times the volume of the surface goblet cells [2,5,11]. However, other evidence indicated that mucous and serous glands also express MUC5AC [12,13]. MUC5AC and MUC5B are also expressed predominantly by club cells in normal and asthmatic airways of mouse and human [3,5,14–16]. While the precise molecular mechanisms are not fully understood, investigations have demonstrated multiple molecular mechanisms of airway MUC5AC production. Interleukin (IL)-13 increases expression of *MUC5AC* in human airway epithelial cells and murine models of asthma through sequential activation of signal transducers (e.g., Janus kinase 1, signal transducer and activator of transcription 6) [2,17]. Epidermal growth factor receptor (EGFR) signaling also induced *MUC5AC* via phosphoinositide 3-kinase (PI3K)-transmembrane protein 16A signaling pathway [18]. In contrast, Foxa2 inhibited by IL-13 signaling negatively regulated *Muc5ac* [17,19]. We also demonstrated that *MUC5AC* expression is regulated, in part, by a cycloocygenase-2 and prostaglandin E2 pathway in human airway epithelial cells [20]. MUC5AC is abundant not only in airways but also in the superficial gastric epithelium [21]. It is also detected in pancreas, colon, gallbladder, and endocervix, and highly associated with various cancers [22].

The nasal epithelium is the first airway barrier between the host and the external environment and largely covered by a mucus gel for upper airway defense. The mucous membranes, or mucosa, lining the nasal airways consist of two layers: the surface epithelium

and the underlying lamina propria which is connective tissue rich in subepithelial glands and blood vessels [23]. Goblet cells in the respiratory epithelium lining the proximal septum and subepithelial glands under respiratory (seromucoss glands) and olfactory epithelium (Bowman's glands) are cellular source of nasal mucus [5]. Gel-forming mucin in human nasal mucous glands are mainly MUC5B and MUC19 while MUC2 and MUC5AC are secreted from both mucous and serous glands [12,13,24,25]. Submucosal glands in tracheobronchi were increased in number and volume in smokers relative to non-smokers and extended to the distal bronchioles in disease conditions such as chronic bronchitis which contributes to the formation of airway plugs [5,26].

Recent investigations have focused on molecular biology underlying single airway mucins. *Muc5ac* transgenic mouse models demonstrated a protective role of against pulmonary influenza virus infection [16] or detrimental roles in allergic airway disease and ventilator-induced acute lung injury [27,28]. However, functions of MUC5AC in other mucus-engaged pulmonary pathogenesis or in nasal airway injury caused by airborne toxicants have not been investigated. The current study was designed to test the hypothesis that MUC5AC is protective in murine models of airway diseases which accompany increased mucus production and/or secretion and enhanced MUC5AC expression. For this purpose, we exposed wild-type mice ($Muc5ac^{+/+}$) and mice genetically deficient in *Muc5ac* ($Muc5ac^{-/-}$) to a pulmonary fibrogen (bleomycin), respiratory syncytial virus (RSV), and subacute ozone (O_3) and compared upper and lower respiratory injury, inflammation, and mucous production/secretion between two mouse genotypes.

MATERIALS AND METHODS

Generation of Muc5ac deficient ($Muc5ac^{-/-}$) mice.

$Muc5ac^{-/-}$ (B6;129-$Muc5ac^{tm1Unc}$/Ehs) mice were generated by targeted deletion of exons 21 to 31 encoding the MUC5AC protein region responsible for glycosylation. A targeting construct consisting of a neomycin-positive and herpes simplex virus thymidine kinase-negative selection cassette (NeoTKXho) in place of an eight kilo-bases (8031 kb) spanning exon 21 to exon 31 of the *Muc5ac* gene (Supplemental Figure S1–A) was made at the National Institute of Environmental Health Sciences (NIEHS). The construct was introduced into embryonic stem cells (ES-E14TG2a) to generate targeted mice at the Mouse Model Core of the University of North Carolina at Chapel Hill (Supplemental Figure S1–A). The targeted ES cells were identified by Southern blot analysis and injected into C57BL/6J mice blastocysts which were transplanted into pseudo-pregnant females. The chimeric offspring obtained were then bred to C57BL/6J mice and the pups screened by Southern blotting. Heterozygous ($Muc5ac^{+/-}$) mice were transferred to the NIEHS animal care facilities and backcrossed into C57BL/6J mice for eight generations to produce whole body knockout mice and wild-type controls (C57BL/6J-129Ola, $Muc5ac^{+/+}$). $Muc5ac^{+/+}$ and $Muc5ac^{+/+}$ mice were identified by Southern blotting (Supplemental Figure S1–B), PCR (Supplemental Figure S1–C), immunohistochemical analyses (Supplemental Figure S2–A to C), and Western blotting (Supplemental Figure S2–C). Pathogen-free breeding colonies of $Muc5ac^{+/+}$, $Muc5ac^{+/+}$, and $Muc5ac^{+/-}$ mice were maintained in sterilized, filter-topped cages and

fed autoclaved food (NIH_31) at the NIEHS animal facilities. All animal use was approved by the NIEHS Animal Care and Use Committee.

Animal experiments.

Male, adult (6-8 weeks old) *Muc5ac*$^{+/+}$ and *Muc5ac*$^{-/-}$ mice were used for all studies. Mice were randomly assigned to the experimental groups. For pulmonary fibrosis endpoints, mice were anesthetized with isoflurane (2% in air) and a single dose (0.5 U/Kg body weight, b.w.) of bleomycin sulfate (Sigma Chemical Co., St. Louis, MO) or vehicle (PBS) was delivered by oropharyngeal aspiration (intratracheal, IT). Mice were sacrificed at 3, 7, or 14 days post-bleomycin. For the RSV disease model, mice were anesthetized with isoflurane and intranasally infected with 10^6 plaque forming units of human RSV-19 strain (ViraSource, Durham, NC) in 50 μl HBSS. HBSS containing Hep-2 cell lysates (50 μl) was intranasally instilled into control mice as vehicle. Animals were sacrificed at 1, 3, 5, or 7 day(s) after intranasal instillation. To evaluate airway O_3 toxicity, mice were placed in individual stainless-steel wire cages within a whole-body inhalation chamber (Hazelton 1000; Lab Products, Maywood, NJ) with free access to water and foods and exposed continuously to 0.3 parts per million (ppm) O_3 for 48 or 72 hr under constant chamber air temperature (72 ± 3°F) and relative humidity (50 ± 15%) as described in detail previously [29]. Parallel exposure to room air was done in a separate chamber for the same duration. All mice were euthanized by sodium pentobarbital overdose (104 mg/Kg body weight) for necropsy immediately after the end of designated exposure. Body fat of mice was measured at 6, 9, and 12 months of age using a dual energy x-ray absorptiometry (Lunar PIXImus, GE Lunar Corp, Chicago, IL).

Brottchoalveolar lavage (BAL) analyses.

The right lung of each mouse was lavaged *in situ*, four consecutive times with HBSS (0.5 mL/25 g b.w.). The BAL fluid returns were centrifuged (1000 *g*, 10 min). An aliquot of the 1st BAL return supernatants (50 μl) were analyzed for total protein concentration (a marker of edema) in Bradford reagent (Bio-Rad, Hercules, PA) as indicated in the manufacturer's procedure. Cell pellets from all lavage returns were combined and resuspended in 1 mL HBSS for epithelial and inflammatory cell counts as reported previously [30]. To detect cell lysis and toxicity, colorimetric assay for lactate dehydrogenase (LDH) was also performed in aliquots (25 μl) of BAL supernatants by determination of NADH production from added NAD+ (Sigma, St. Louis, MO).

Sandwich enzyme-linked immunosorbent assay (ELISA).

BAL supernatants (25 μl) were used to determine neutrophil myeloperoxidase (MPO) using a mouse-specific ELISA kit (R&D Systems, Minneapolis, MN) according to manufacturer instructions. Secreted MUC5AC protein was also determined in BAL supernatants following the published method [29]. Briefly, an aliquot of BAL supernatant (20 μl) was loaded in each well of an ELISA plate containing a goat polyclonal anti-MUC5AC capture antibody (1:40 dilution of sc-16903; Santa Cruz Biotechnology Inc., Dallas, TX) in pH 9.5 bicarbonate-carbonate coating buffer (BD OptEIA Reagent; BD Biosciences, San Diego, CA). The plate was incubated at 48°C until the reaction was dry (>5 hr). The wells were washed and blocked overnight with an assay diluent containing 10% fetal bovine serum (BD Opt EIA) at

4°C. The samples were then incubated with a biotinylated monoclonal anti-MUC5AC detection antibody (1:100 of Clone 45M1, Thermo Scientific, Waltham, MA) for 1.5 hr at 37°C. Following incubation with a peroxidase-conjugated secondary antibody (1:2500, goat anti-mouse-IgG-HRP), color change was developed by adding the TMB substrate solution (BD Biosciences). Optical density was measured at 450 nm after the stop buffer was added.

Lung and nasal airway histopathology and immunohistochemistry.

The left lung from each mouse was inflated intratracheally *in situ* with 10% neutral buffered formalin, and fixed following procedures published previously [31]. The fixed lung lobe was sectioned at proximal (generation 5) and distal (generation 11) levels of the main axial airway[32]. The excised heads of mice from RSV and O_3 studies were flushed retrograde via a cannula through the nasopharyngeal orifice with 10% neutral buffered formalin. The fixed heads were processed for decalcification and the proximal aspect of the nasal cavity section (i.e., at the level of upper incisor teeth, T1) was cut following procedures published previously [33]. The lung and nasal tissue blocks were embedded in paraffin, and 5 μm-thick section cuts were stained with hematoxylin and eosin (H&E) for histopathological analysis, with Alcian Blue (pH 2.5)/periodic acid-Schiff (AB/PAS) reagent for acidic and neutral mucus detection, and with Mason's trichrome for collagen localization. Severity of histopathologic lung toxicity in the bleomycin study was determined by blinded microscopic evaluation of H&E-stained slides for inflammation and injury and Masson-trichrome-stained slides for collagen associated with areas of inflammation (Experimental Pathology Labs, Morrisville, NC). Tissues were also stained by immunohistochemical methods using mouse monoclonal (IgG_1) anti-MUC5AC (1:100 dilution of Clone 45M1, Thermo Fisher Scientific, Waltham, MA), rabbit anti-MUC2 (1:667 dilution of GTX100664, GeneTex, Irvine, CA), goat anti-RSV (1:200 dilution of ab20745, Abeam, Cambridge, MA), and proliferating cell nuclear antigen (1:200 dilution of PCNA; sc-56, Santa Cruz Biotechnology). Briefly, deparaffinized and hydrated tissue sections on microscope slides were treated sequentially with antigen unmasking solution (Vector Laboratories, Burlingame, CA), 0.1% proteinase K, 1N HC1 (1 hr for PCNA only), and endogenous peroxidase quenching solution (5% H_2O_2) before blocking with 1.5% serum (Vectastain ABC kits, Vector Laboratories) at room temperature. Tissue sections were then incubated overnight at 4°C with each specific primary antibody. After incubation with proper biotinylated secondary antibodies (1:200, Vectastain ABC kits) and Avidin/Biotin solution, antigens were detected by 3,3'-diaminobenzidine-peroxidase substrate solution (1 min for PCNA, 5 min for RSV, 10 min for others, Sigma), and slides were mounted with cover glasses after counterstaining, if necessary, and dehydration. For immunofluorescence staining of RSV, micrograph slides incubated with primary antibody were incubated overnight with fluorochrome-conjugated goat IgG solution (1 μg/mL) for 1 hr and cover-slipped with prolong Gold Antifade reagent with DAPI (Thermo Fisher Scientific). Nasal airways and lungs from a subset of male mice (22 *Muc5ac*$^{+/+}$, 23 *Muc5ac*$^{-/-}$) at 11-12 months were processed for H&E and AB/PAS staining as indicated above. Occurrence of preinvasive alveolar epithelial proliferation was determined by percent of mice with increased focal cellularity in alveoli including early adenoma on H&E-stained light micrographs. Nodular lymphocytic accumulation was determined by percent of mice bearing lymphocyte nodules in perivascular-peribronchial pulmonary regions on H&E-stained light micrographs.

Morphometric analysis of nasal airway mucosubstances and terminal bronchial proliferating cells.

The amount of AB/PAS-stained mucosubstances in nasal airways from RSV and O_3 studies was estimated using computerized image analysis and standard morphometric techniques [33,34]. Briefly, images of AB/PAS-stained cross-sections from the proximal nasal airway (turbinate section T1) were taken using a light microscope with an attached camera and software (Olympus BX53 and cellSense, Olympus, Center Valley, PA). The AB/PAS-positive areas within the surface epithelium lining mid-septum and ventral septum (from the tip level of nasoturbinate to the bottom of the ventral septum) was calculated from the semi-automatically circumscribed perimeter of the stained material using the NIH Image J 1.52a software (https://imagej.nih.gov/ij/index.html). The length of the basal lamina underlying the surface epithelium was concomitantly calculated from the contour length on digitized images using the same system. Similarly, stored PAS-positive substances in subepithelial glands (mucous glands) in the ventral septum (from the bottom level of maxilloturbinate to the end of the ventral septum) was quantitated and normalized to the length of basal lamina on top of the lamina propria. The volume of intraepithelial mucosubstances per unit surface area (volume density, Vs, nl/mm^2 basal lamina) was determined as previously described in detail[35]. Areas of PAS-positive secretion in the ventral wall region of proximal nasal sections from the O_3 study were also measured as indicated above.

In situ hybridization (ISH) of airway mucins.

Expression of *Muc4* and *Muc5b* transcripts in lung and nasal tissues was detected by *in situ* RNA detection techniques in accordance with manufacturer instructions (FFPE assay kit; Advanced Cell Diagnostics, Newark, CA). Briefly, formalin-fixed paraffin-embedded tissue sections on charged slides were baked at 60°C (1 hr for lung, overnight for nasal) and deparaffinized and rehydrated. The sections were pretreated with hydrogen peroxide, incubated in boiling Target Retrieval solution for 15 min, and permeabilized with Protease Plus solution (40°C, 30 min for lung, 15 min for nasal). Tissues were then hybridized with labeled double z RNA probe pairs specific for mouse *Muc4* and *Muc5b* (40°C for 2 hr). The target mRNA signals were sequentially amplified using a horseradish peroxidase-based signal amplification system and color development was detected with 3,3′-diaminobenzidine. The slides were counterstained with hematoxylin for 10 sec. Representative light photomicrographs were prepared by Olympus microscope BX53 and cellSense software (Central Valley, PA).

Lung RNA isolation and polymerase chain reaction (PCR).

Total lung RNAs were isolated from lung homogenates (RNeasy Mini Kit, Qiagen Inc., Valencia CA), and reverse transcribed into cDNAs. Aliquots of cDNA (40 ng) were subjected to quantitative PCR with mouse-specific primers for *Muc5ac* (amplifying nucleotide 3547-3667 of NM_010844; 5'-TGCATGCGTACCTGCCAGAA-3', 5'-CACACTGCATTGTGCCCTCA-3'), *Muc5b* [36], *Muc4* (RealTimePrimers, Melrose Park, PA), and *Muc2* [36], and 18s ribosomal RNA, an internal control (amplifying nucleotide 324-507 of K1364; 5'-TACCTGGTTGATCCTGCCAG-3', 5'-CCGTCGGCATGTATTAGCTC-3') using CFX Connect Realtime System (Bio-Rad). Copy

number of RSV nucleoprotein (N) was determined by droplet digital PCR (ddPCR). Briefly, an aliquot of lung cDNA (2 ng) in PCR mixture containing a SYBR Green dye (Bio-Rad) and 125 nM of RSV N gene primers (amplifying nucleotide 1137-1220 of M11486; 5'-AGATCAACTTCTGTCATCCAGCAA-3', 5'-TTCTGCACATCATAATTAGGAGTATCAAT-3') was partitioned into approximately 20,000 individual nanoliter-sized water-in-oil droplets by Bio-Rad QX200 Automated Droplet Generator followed by PCR reaction (C1000 Touch Thermal Cycler, Bio-Rad). The droplets were then read one-by-one in QX200 Droplet Reader (Bio-Rad) and assigned as positive (1) or negative (0). The copy number of the N gene per μg RNA was calculated by the positive droplets.

Western blot analyses.

Protein level of epithelial cadherin (E-cadherin, 120/80 kDa), an intercellular adherens junction protein in epithelial barrier, was determined. Total lung proteins were isolated from individual mouse lung homogenate in radioimmunoprecipitation assay buffer (n = 4/group) and equal amounts of the lung proteins from two mice were pooled. Aliquots of pooled proteins (70-150 μg) were separated on Tri-HCl SDS-PAGE genes (7.5% or 10-20%, Bio-Rad) and analyzed by routine Western blotting using specific antibodies (Santa Cruz Biotechnology) against E-cadherin (sc-59778, 1:200 dilution) and pan-actin (sc-1616, 1:500 dilution). Blot images were scanned using the FluorChem HD2 System (ProteinSimple, San Jose, CA) and quantified by densitometry using Image J Gel analysis software (https://imagej.nih.gov).

Sircol assay for lung collagen quantitation.

Total soluble collagen content in right lungs was determined using the Sircol collagen-dye binding assay kit (Biocolor, Carrickfergus, N. Ireland). Briefly, whole right lung lobes from each mouse were homogenized in 1 mL of acetic acid solution (0.5 N with protease inhibitors) and incubated on a gentle shaker overnight at room temperature. The acid extracts were centrifuged (15,000g for 30 min) and aliquots of the supernatants (200 μl) containing acid-soluble collagens were mixed with 1 mL Sirius Red dye reagent for 30 min on a shaker (800 rpm). The pellets (bead-dye-collagen complex) acquired by centrifugation (10,000g for 10 min) were dissolved in 1 ml alkali reagent (0.5 M NaOH). Absorbance of alkali reagent in which collagen-dye complex was dissolved was measured at 550 nm. The amount of collagen was quantitated using a standard curve prepared from collagen standard.

Serum immunoglobulin E (IgE) detection.

From each mouse, an aliquot of serum (1 μl) was isolated from blood samples collected by cardiac puncture and was diluted in an assay diluent (1:100). IgE levels were determined using a mouse-specific sandwich ELISA kit (BD Opt EIA) and similarly prepared serial dilution of IgE standards (BD Biosciences).

Statistics.

Data were expressed as the group mean ± standard error of the mean (SEM). Two-way analysis of variance (ANOVA) was used to evaluate the effects of genotype (*Muc5ac*$^{+/+}$ vs.

Muc5ac$^{-/-}$) and exposure (RSV vs vehicle, bleomycin vs vehicle, O_3 vs air) at each time point. One-way ANOVA was used to assess MUC5AC secretion or *Muc5ac* mRNA expression in *Muc5ac*$^{+/+}$ mice. Kruskal-Wallis ANOVA on Ranks test was applied to the histology score data. The Student-Newman-Keuls test was used for *a posteriori* comparisons of means for all multiple comparisons ($P < 0.05$). All statistical analyses were performed using SigmaPlot 13.0 program (Systat Software, San Jose, CA).

RESULTS

Enhanced responsivity of *Muc5ac*$^{-/-}$ mice to bleomycin-induced pulmonary injury and fibrosis

The b.w. gain at 14 days after bleomycin treatment was significantly lower in *Muc5ac*$^{-/-}$ mice compared to *Muc5ac*$^{+/+}$ mice (Figure 1–A). Relative to respective controls, bleomycin significantly increased the BAL protein concentration (a marker of protein edema), LDH activity (a marker of cell death), and the numbers of total cells and leukocytes (neutrophils and lymphocytes) in *Muc5ac*$^{+/+}$ and *Muc5ac*$^{-/-}$ mice (Figure 1–B to F). However, bleomycin-induced protein edema and lung cell death (7-14 days) as well as numbers of lung leukocytes (3-14 days) in *Muc5ac*$^{-/-}$ mice were significantly greater than those in *Muc5ac*$^{+/+}$ mice (Figures 1–B to F).

Histopathologic analysis found that bleomycin caused sporadic fibrotic patches in parenchyma with predominant fibrogenesis in perivascular-peribronchial regions from 7 days and more widespread fibrosis at 14 days post-bleomycin in both genotypes (Figure 2). Relative to *Muc5ac*$^{+/+}$ mice, the magnitude of the bleomycin-induced fibrosis was more severe and widespread in *Muc5ac*$^{-/-}$ mice at 7-14 days (Figure 2). Histopathologic scores of inflammation and fibrosis as well as lung soluble collagen contents (collagens type I-V) were significantly higher in *Muc5ac*$^{-/-}$ mice than in *Muc5ac*$^{+/+}$ mice at 14 days (Figure 3–A). In *Muc5ac*$^{+/+}$ lung, *Muc5ac* mRNA abundance (3 days) and airway secretion (7 days) were significantly enhanced by bleomycin (Figure 3–B). E-cadherin levels determined as an intercellular junction marker were significantly lower in vehicle (PBS)-treated*Muc5ac*$^{-/-}$ mice than in vehicle-treated *Muc5ac*$^{+/+}$ mice (Figure 3–C). Bleomycin treatment significantly decreased amounts of mature lung E-cadherin (80 kDa) in both genotypes of mice but more markedly in *Muc5ac*$^{-/-}$ mice than in *Muc5ac*$^{+/+}$ mice at 3 and 14 days (Figure 3–C).

Bleomycin caused mucous (goblet) cell metaplasia (MCM) in *Muc5ac*$^{+/+}$ and *Muc5ac*$^{-/-}$ mice at 7 and 14 d (Figure 4–A). Microscopic analysis indicated that MUC5AC proteins were localized in goblet cells of bronchi and bronchioles after vehicle or bleomycin in *Muc5ac*$^{+/+}$ mice and were not detected in *Muc5ac*$^{-/-}$ mice (Figure 4–A, insets). Although basal level of AB/PAS-stained bronchial intraepithelial mucus was relatively scarce in *Muc5ac*$^{-/-}$ lungs compared to *Muc5ac*$^{+/+}$ lungs, the overall magnitude of bleomycin-induced MCM was greater in *Muc5ac*$^{-/-}$ lungs than in *Muc5a*$^{+/+}$ lungs as MCM was more widely extended to smaller airways adjacent to fibrotic regions (at 14 days) in *Muc5ac*$^{-/-}$ mice compared to *Muc5a*$^{+/+}$ mice (Figure 4–A), suggesting a compensatory increase of non-MUC5AC mucin in *Muc5ac*$^{-/-}$ airways. Expression of MUC2 protein, *Muc5b* mRNA, and *Muc4* mRNA were determined as these mucins were known to increase in pathologic

airways [37–39] and compensate for *Muc5ac* deficiency [15,36,40,41]. ISH detected *Muc4* and *Muc5b* mRNAs in vehicle-treated bronchial epithelium of both genotypes (Figure 4–A). Bleomycin increased *Muc4* and *Muc5b* transcripts in bronchial-to-bronchiolar epithelium of fibrogenic regions and their increase was co-localized with MCM throughout the conducting airways (Figure 4–A). High *Muc4* expression was detected in honeycombing alveoli of *Muc5ac*$^{-/-}$ mice at 14 days post-bleomycin and it was minimal throughout epithelium at 7 days post-bleomycin (Figure 4–A). Induced expression of *Muc4* and *Muc5b* mRNA markedly in proximal-to-distal conducting airway epithelium was higher in *Muc5ac*$^{-/-}$ mice than in *Muc5ac*$^{+/+}$ mice at 7-14 days, indicating compensatory overexpression (Figure 4–A). Immunohistochemical staining found that MUC2 proteins were constitutively expressed in AB/PAS-positive bronchial-to-bronchiolar epithelium of both strains and it was increased by bleomycin in *Muc5ac*$^{-/-}$ mice at 7 days (Figure 4–A). qPCR detected significantly greater expression of *Muc5b* (14 days), *Muc4* (7 and 14 days), and *Muc2* (3 days) messages in *Muc5ac*$^{-/-}$ mice than in *Muc5ac*$^{+/+}$ after bleomycin treatment (Figure 4–B). Upregulation of *Muc2* mRNA by bleomycin treatment preceded (at 3 days) the increase of MUC2 proteins (at 7 days) in *Muc5ac*$^{-/-}$ mice (Figures 4–A and B). Overall, these results indicated that MUC4 and MUC5B together with MUC2 contribute to bleomycin-induced MCM in *Muc5ac*$^{-/-}$ mice.

Enhanced sensitivity of *Muc5ac*$^{-/-}$ mice to RSV

Lung injury by RSV—RSV infection caused significant airway inflammation and bronchial and bronchiolar epithelial hyperplasia and hyperproliferation in *Muc5ac*$^{+/+}$ and *Muc5ac*$^{-/-}$ mice (Figure 5–A). Large syncytia (a multinucleated cell resulted from fusions of uninuclear cells by infected RSV) formation was more evident in lungs from *Muc5ac*$^{-/-}$ mice (Figure 5–A, arrow heads). Compared to *Muc5ac*$^{+/+}$ lungs, RSV-induced increases in the numbers of BAL epithelial cells and the concentration of neutrophilic myeloperoxidase (MPO) were significantly greater in *Muc5ac*$^{-/-}$ lungs at 1-day post-RSV (Figure 5–B). Consistent with more severe airway epithelial hypertrophy/hyperplasia and smooth muscle thickening (Figure 5–A, arrows), serum IgE level was significantly higher in *Muc5ac*$^{-/-}$ mice than in *Muc5ac*$^{+/+}$ mice at 5 days post-RSV (Figure 5–C).

Immunohistologic localization of RSV indicated that viral proteins were predominantly in pleura, conducting airway epithelium, and blood vessels at 1-day post-RSV and more severe viral pleuritis was found in *Muc5ac*$^{-/-}$ mice than in *Muc5ac*$^{+/+}$ mice (Figure 6–A). By 3 days post-RSV, virus diffused throughout the lung parenchyma in both genotypes, but infection diminished by 5 days (Figure 6–A). There was little difference in the magnitude of lung RSV localization between two genotypes at 3 and 5 days (Figure 6–A), suggesting that Muc5ac may contribute to a barrier against RSV in early stages of viral entry and spread. Corresponding to RSV immunohistochemistry, viral nucleoprotein (N) gene copy number was significantly higher in *Muc5ac*$^{-/-}$ lung than in *Muc5ac*$^{+/+}$ lung at 1-day post-RSV but not at later times (Figure 6–B).

The amount of mature E-cadherin protein (80 kDa) was basally lower in vehicle-treated *Muc5ac*$^{-/-}$ mice than in vehicle-treated *Muc5ac*$^{+/+}$ mice (Figure 6–C). After 1 and 3 day(s) post-RSV, 120 kDa (mature)/135 kDa (precursor) E-cadherin level was detected in *Muc5ac*

$^{+/+}$ lungs, which was declined at 5 days post-RSV in these mice (Figure 6–C). E-cadherin was barely detected in *Muc5ac*$^{-/-}$ lungs after RSV infection (Figure 6–C).

Nasal Airway Injury by RSV—Immunohistochemical localization in cross sections of the proximal nasal turbinate (T1) indicated that RSV was mainly in surface epithelium lining septum, maxilloturbinate, blood vessels, and subepithelial glands in septum and walls, and walls at 1-day post-RSV (Figure 7). As found in the lung, RSV was most extensively detected at 3 days when nasal airway injury peaked, and virus propagation was relatively resolved at 5 days (Figure 7). RSV was more intensely and diffusively localized in *Muc5ac*$^{-/-}$ mice than in *Muc5ac*$^{+/+}$ mice at 1 day, and nasal airway injury indicated by epithelial sloughing and hyperplastic changes in medial meatus region (medial wall, nasoturbinate, maxilloturbinate) was more prevalent in *Muc5ac*$^{-/-}$ mice than in *Muc5ac*$^{+/+}$ mice at 1-5 day(s) post-RSV (Figure 7).

AB/PAS staining of nasal airway epithelium revealed mucous cell hyperplasia in the mid-septum of *Muc5ac*$^{+/+}$ mice from 1-day post-RSV (Figure 8–A, B). Relative to vehicle control, RSV infection increased MUC5AC protein expression mostly in AB/PAS-positive nasal respiratory epithelium (mid- and ventral septum) and some in Bowman's glands in *Muc5ac*$^{+/+}$ mice (Supplemental Figure S3–A). H&E staining found that RSV infection caused most morphological changes including epithelial sloughing and hypertrophy at 3 days post-infection largely in mid-septum, maxilloturbinate, and lateral meatus wall, and the injury was greater in *Muc5ac*$^{+/+}$ mice than in *Muc5ac*$^{-/-}$ mice (Figure 8–A, mid-septum shown). While basal levels of AB/PAS-positive goblet cells were relatively fewer in *Muc5ac*$^{-/-}$ mice, RSV also caused significant goblet cell hyperplasia in *Muc5ac*$^{-/-}$ mice at later (7 days) post-infections days (Figure 8–A, B). Interestingly, increase in PAS-positive substances in submucosal glands (mostly mucous glands) was more prevalent in *Muc5ac*$^{-/-}$ mice than in *Muc5ac*$^{+/+}$ mice after RSV infection (Figure 8–A). RSV-induced cellular proliferation and injury indicated by proliferating cell nuclear antigen (PCNA) immunostaining were greater in *Muc5ac*$^{-/-}$ turbinates than in *Muc5ac*$^{+/+}$ turbinates (Supplemental Figure S3–B). Consistent with the subepithelial gland hyperplasia (increased grand volume), PCNA localization in RSV-infected *Muc5ac*$^{-/-}$ turbinates was predominant in subepithelial gland cells in ventral septum (Figure S3–B). Immunohistochemical staining of MUC2 (Supplemental Figure S3–C) and *in situ* hybridization of *Muc5b* mRNA (Supplemental Figure S3–D) found that overall nasal expression of MUC5B and MUC2 may be increased by RSV infection similarly in both genotypes. *Muc5b* mRNA was detected mainly in hyperplastic/metaplastic respiratory epithelium (goblet cells and other cells) lining septum, nasoturbinate, and ventral wall and less frequently in Bowman's glands (Supplemental Figure S3–D). It was, however, seldom detected in subepithelial glands. In contrast, MUC2 protein was increased in seromucosal glands in septum and lateral wall and in Bowmans' glands with minor localization in septal surface epithelium (Supplemental Figure S3–C). *Muc4* mRNA was detected only in cells surrounding maxillary sinus of the nasal airways (data not included). Therefore, compensatory septal goblet cell hyperplasia and submucosal gland hyperplasia manifest in *Muc5ac*$^{-/-}$ nasal airways may be at least in part contributed by upregulated MUC5B and MUC2, respectively.

Analyses of electron micrographs of the vehicle control epithelium from T1 found reduced mucus storage in goblet cell vesicles of *Muc5ac*$^{-/-}$ mice as indicated by relatively empty granules and electron-dense central core compared with the granule features in *Muc5ac*$^{+/+}$ mice (Figure 8–C). After 1-3 day(s) of RSV infection, swollen granules, exocytosis, and formation of vacuoles were evident in goblet cells and trapping of virus infection-associated debris in fused granules undergoing exocytosis were more commonly detected in wild-type mice (Figure 8–C). However, *Muc5ac*$^{-/-}$ septum was less marked in these goblet cell activities after virus infection (Figure 8–C). In contrast to the surface goblet cells, subepithelial glands in septum of *Muc5ac*$^{-/-}$ mice presented uniformly-stained and electron-dense granules connected with rich rough endoplasmic reticulum at 3 days post-RSV, while RSV-infected glandular vesicles in *Muc5ac*$^{+/+}$ septum had particularly electron-lucent outer rim (Figure 8–C).

Increased O_3 -induced injury in nasal turbinate and centriacinar region of *Muc5ac*$^{-/-}$ mice

Exposure to 0.3-ppm O_3 caused epithelial exfoliation in mid- and dorsal-septum, mucous cell hyperplasia throughout the septal respiratory epithelium, mucoserous gland proliferation and hyperplasia, and blood vessel congestion in nasal airways of both genotypes from 48 hr (Figure 9–A). Subepithelial gland expansion and congestion accompanying hypertrophy of basal lamina beneath septum, nasal wall, and turbinate were greater in *Muc5ac*$^{-/-}$ mice than in *Muc5ac*$^{+/+}$ mice at 48 hr exposure (Figure 9–A). While O_3 significantly increased AB/PAS-positive intraepithelial substances in mid-septum only in *Muc5ac*$^{+/+}$ mice, PAS-positive stored mucoserous gland substances were significantly higher in *Muc5ac*$^{-/-}$ mice than in *Muc5ac*$^{+/+}$ mice basally and after O_3 (Figure 9–B). In addition, these changes corresponded with the O_3-induced secretion of PAS-positive mucosubstances in ventral wall detected only in *Muc5ac*$^{-/-}$ mice (Figure 9–B). Using *in situ* hybridization, we found that O_3 markedly increased *Muc5b* mRNA (peak at 48 hr) mainly in respiratory epithelium undergoing goblet cell hyperplasia (lining septum, nasoturbinate, and ventral wall) and less frequently in Bowman's glands in both genotypes of mice (Figure 9–C). However, *Muc5b* was seldom expressed in subepithelial glands, indicating other mucin genes/proteins (e.g., *Muc2, Muc7*) may involve in PAS-positive subepithelial gland hyperplasia and secretion in *Muc5ac*$^{-/-}$ mice.

MCM developed in bronchial epithelium after O_3 exposure (peaked at 48 hr) was predominant in *Muc5ac*$^{+/+}$ mice relative to that in *Muc5ac*$^{-/-}$ mice (Figure 10–A). In contrast, O_3-induced injury and proliferation in the centriacinar region (junction of terminal bronchiole and alveoli) as determined by the abundance of PCNA-positive S phase cells were markedly higher in *Muc5ac*$^{-/-}$ mice than in wild-type mice at 72 hr (Figure 10–B). Total protein concentration and total cells (Figure 10–C) as well as inflammatory (macrophages, neutrophils, lymphocytes) and epithelial cell numbers in BAL were, however, not significantly different between two genotypes of mice after 48-72 hr exposure to O_3. Lung E-cadherin amount detected at 120 (mature)/135 (precursor) kDa was basally lower in air-exposed *Muc5ac*$^{-/-}$ mice than in air-exposed *Muc5ac*$^{+/+}$ mice (Figure 10–D). O_3 exposure decreased E-cadherin proteins in *Muc5ac*$^{+/+}$ mice, and E-cadherin levels in *Muc5ac*$^{+/+}$ mice remained lower in *Muc5ac*$^{-/-}$ mice than after O_3 exposure (Figure 10–D).

Discussion

The current investigation demonstrated that deficiency of *Muc5ac* increased susceptibility to acute injury caused by virus and xenobiotics in nasal and pulmonary airways of mice. Compared to wild-type mice, significantly greater bleomycin-induced lung inflammation and fibrosis, early RSV infection and RSV-induced nasal and pulmonary injury, and O_3-induced nasal mucosal and centriacinar pulmonary injury were found in *Muc5ac*$^{-/-}$ mice. Adaptive or augmented compensatory epithelial MCM in *Muc5ac*-deficient mice was concurrent with increased *Muc4* mRNA, *Muc5b* mRNA, and/or MUC2 during pulmonary fibrogenesis. Lack of *Muc5ac* also led to subepithelial gland hypertrophy/hyperproliferation and/or hypersecretion in nasal airways after RSV and O_3 exposure. A marker of epithelial barrier, E-cadherin, was suppressed in *Muc5ac*-deficient mice basally and after bleomycin, RSV, and O_3 exposure. Results thus demonstrated requirement of MUC5AC for airway defense against acute phase injury and the compensatory adaptation of airway mucin system.

In disease conditions such as chronic bronchitis which contributes to the formation of airway plugs, submucosal glands in tracheobronchi increased in number and volume in smokers relative to non-smokers and extended to the distal bronchioles [26]. In addition, total tracheobronchial gland volume in lungs from severe COPD and chronic bronchitis patients or serous gland substance secretion in asthmatic lungs were 4-fold higher than those in healthy lung [5,42]. Our findings particularly in RSV- and O_3-susceptible *Muc5ac*-deficient mice were consistent with these observations. Hyperplasia of the PAS-positive mucous glands and appearance of AB/PAS-positive submandibular-like glands (with mixed histologic feature of serous and mucous glands) were more distinct in *Muc5ac*$^{-/-}$ mice infected with RSV or exposed to O_3. We postulate that *Muc5ac*$^{-/-}$ mice bearing decreased number of airway surface goblet cells and their granule contents may facilitate enrichment of mucus and/or serous substances in submucosal gland acini for their compensatory mucosal defence.

While produced little in healthy bronchial airways, MUC5AC has been a marker of MCM [43,44] and is highly increased in asthma, allergic airway disorder, and acute lung injury [28,45–48]. A *MUC5AC* single nucleotide polymorphism (SNP, rs1132440) was significantly associated with respiratory outcomes (bronchitis, wheeze, asthma, hay fever) [49]. A direct correlation was also found between the polymorphism-related length of the MUC5AC variable number tandem repeat fragment and the severity of cystic fibrosis [50]. Our results are consistent with the hypothesis that lack of *Muc5ac* may lead to porous barrier during airway pathogenesis, which is not able to retain protective molecules in mucosa and in cells by trapping foreign bodies to inhibit acute phase of epithelial injury, viral entry into tissues, inflammation, and fibrogenesis. During RSV infection, the reduction in mucus levels in *Muc5ac*$^{-/-}$ mice may allow virus to reach the cell surface or viral products could diffuse through the mucus. Overexpression of *Muc5ac* provided resistance to pulmonary influenza virus infection and neutrophilia [16], which was consistent with our current findings in the RSV disease model. *Muc5ac*-overexpressing mice had 20-fold increased lung MUC5AC protein but preserved mucociliary clearance function as the increased MUC5AC expanded (thicker), not concentrated, the mucus layer [16]. The anti-influenza role of MUC5AC was proposed to be at least in part by biochemical competition of viruses with host-derived

materials for interaction with the oligosaccharide-attached terminal groups (e.g., sialic acid, fucose, sulfate) of MUC5AC [51,52]. The sequence, conformation, and charges of these mucin sugar epitopes are known to modulate pathogen adhesion, and recognition and domains of the protein core can also serve as ligands [53,54]. Considering multiple antiviral substances including β-defensin, lactoferrin, and type I and III interferons against viral infection in airway mucus layer [55], the more rapid and widespread effects of RSV infection in *Muc5ac* $^{-/-}$ mice are predicted due to reduced mucus during the early infection period. The functional role for the airway MUC5AC studied using transgenic animal models, however, has been debatable. For example, *Muc5ac* deletion improved survival time and decreased lung edema, inflammation, and gas-exchange reduction against ventilator-induced acute lung injury [28]. *Muc5ac*$^{-/-}$ mice had significantly reduced MCM and mucous plugging, and airway hyperreactivity response in an allergic airway disease model [27], consistent with the association of *MUC5AC* to bronchoconstriction of asthmatics [45]. Overall, the relationship between MUC5AC and airway pathogenesis is likely complex, and it may vary depending on the damaged area/cell type and the severity of mucus production/secretion in the diseases.

Basal, ciliated, and type 2 cells have been widely studied as potential stem/progenitors of metaplastic goblet cells during the pathogenesis of airway disorders. Signal transduction pathways including EGFR-PI3K/Akt (ciliated apoptosis inhibition), interleukin-13 recetptor-STAT6 (ciliated cell mucus production), and Notch2 (basal cell to goblet cell) have been demonstrated to involve the MCM[56–59], and trans-differentiation (lineage reprogramming) may underlie the cellular level of goblet cell formation in the fully differentiated respiratory epithelium (e.g., club cell, ciliated cell). Recent investigations on progenitor cells have focused on club cells which are ubiquitous throughout the conducting airways of mice while restricted to the distal bronchioles in humans [11]. Club cells possess the entire secretory machinery to ensure post-translational maturation of mucins and populate the large and small murine airways [14] Murine club cells are also found to be the major sources of MUC5B and MUC5AC [15,60]. Supporting these findings, mice that overexpress *Muc5ac* under control of club-cell secretory protein gene (*Ccsp, Cc10*, or *Scgblal*) produced more MUC5AC without goblet cell hyperplastic or metaplastic changes and evidence of mucin granules were detected in the club cells [16]. Presence of cells sharing the characteristics of goblet cells and club cells in asthmatic mouse airways, which do not exist in normal murine epithelium, [61] and decrease in club cells in allergen challenged airway further supported club cells as progenitor [62]. We also determined marked increase of epithelial mucin messages (*Muc5b, Muc4*) or protein (MUC2) throughout the conducting airways including small bronchioles and terminal bronchioles, indicating production of these mucins in the club cells in response to environmental stimuli. However, lack of AB/PAS staining in the mucin-positive distal airway epithelium of the fibrotic lung in the current and previous studies [14,16] requires further investigation.

Previous work indicated that *Muc5ac* deficiency was compensated by an increase in Muc4 in the ocular surface of mice [40] and MUC5AC alteration in cornea of allergic eye disorder was compensated by secretion of MUC1, MUC2, and MUC4 [41]. Compensatory increase of MUC5B in *Muc5ac*$^{-/-}$ mice were also reported in eyes [36]. In tracheobronchial airways, *Muc5b*$^{-/-}$ mice had heightened Muc5ac in goblet cells [15]. MUC2 is a rarely detected mucin in healthy airways but it is associated with asthmatic and COPD patients [37], and MUC4 is

involved in cell proliferation signaling and has been a marker of various cancers including lung adenocarcinoma [38,39]. We demonstrated that MUC5B and MUC2 (in lung and nasal airways) as well as MUC4 (in lung) may contribute in part to the compensatory increase of mucous cells in airways of injured *Muc5ac*$^{-/-}$ mice. Overall, our results and others indicate that single airway mucin deficiency may affect the composition and quantity of mucus in pulmonary and nasal airways for mucin compensation as an alternative defensive mechanism in airway mucosa.

Results of our experiments supported reduction of lung E-cadherin, an intercellular apical junctional complex (adherens junctions), by bleomycin, RSV or O_3 exposure observed in *Muc5ac*$^{+/+}$ mice. RSV altered the molecular composition of tight junctions leading to airway epithelial hyperpermeability, and decreased expression of tight-junction proteins and accumulation of cleaved extracellular fragments of E-cadherin in BAL [63]. During development of bleomycin-induced pulmonary fibrosis, E-cadherin was downregulated to promote accumulation of myofibroblasts [64] In addition, O_3 caused rapid disruption of lung epithelial barrier followed by increased neutrophilic inflammation and declined tight junction proteins and E-cadherin in mice [65]. A recent study determined that genetic loss of E-cadherin led to airway epithelial damage including epithelial denudation, decreased tight junction (zonula occludens-1) expression, loss of ciliated cells, and spontaneous goblet cell metaplasia in addition to eosinophilic inflammation and enlarged airspace in mice [66]. The authors postulated loss of E-cadherin as a critical step in the development of asthma or emphysema [66].

While further examinations are warranted, we found several severe phenotypes in aged (11-12 months) *Muc5ac*$^{-/-}$ mice than in aged *Muc5ac*$^{+/+}$ mice, which included the increased tendency of body fat (Supplemental Figure S4–A) and compensatory nasal septal mucous cell hyperplasia and nasal submucosal gland hyperplasia (Supplemental Figure S4–B). In addition, *Muc5ac* deficiency caused more severe and/or frequent nodular lymphoid aggregation and preinvasive benign neoplasm indicated by focal spontaneous alveolar hyperplasia or small adenomas (Supplemental Figure S4–C). The *Muc5ac*$^{-/-}$ mice also developed spontaneous gastric antro-pyloric adenoma by age 8-12 months [67] MUC5AC is a commonly detected polymeric mucin in lung adenocarcinoma and was a significant determinant of poor prognosis, especially in patients with *KRAS*-mutant tumors [68]. Different from the enhanced spontaneous preinvasive changes in aged *Muc5ac*$^{-/-}$ lungs and stomachs, chemical-induced lung tumorigenesis was significantly lower in *Muc5ac*$^{-/-}$ mice (BALB/cJ background) compared with that in wild-type mice [68], indicating different underlying molecular mechanisms.

In conclusion, ablation of *Muc5ac* is deleterious in the early response phase of airway inflammation and injury. Lack of *Muc5ac* affected the quantity of mucus and mucus-producing cells at baseline and the composition of mucins during airway pathogenesis. *Muc5ac* deficiency was compensated by other mucins followed by adaptive MCM and submucosal gland hyperplasia as the injury progresses, which explained an alternative defensive mechanism to avoid further mucosal injury in*Muc5ac*$^{-/-}$ mice. While murine models have been useful to investigate MUC5AC in various disorders, differences remain between human and mouse airways in mucin composition and in distribution of potentially

progenitor club cells. In addition, due to the adaptive mechanism of mucin compensation, genetic deletion of a single mucin gene may not be sufficient to address its role in airway pathogenesis. Although MUC5AC is found to be essential for host defense against airway toxicants, overproduction of MUC5AC has deleterious effects as well. Therefore, control of proper mucin induction and mucus secretion may enhance the intrinsic role for mucin in airway protection and defense.

Supplementary Material

Refer to Web version on PubMed Central for supplementary material.

ACKNOWLEDGMENTS

This research was supported by the Intramural Research program of the National Institute of Environmental Health Sciences, National Institutes of Health, Department of Health and Human Services. The authors thank. Dr. Daniel Morgan for coordinating O_3 exposures at the NIEHS Inhalation Facility under contract to Alion Science and Technology, Inc. The authors highly appreciate Mrs. T. Beth Mahler in NIEHS Comparative and Molecular Pathogenesis Branch for her efforts to format and finalize histology images and figures. Mrs. Pamela Ovwigho and Natasha Clayton in the NIEHS Histology Core Laboratory provided excellent histology support, Mrs. Deloris Sutton and Mr. Robert Keys in the NIEHS Electron Microscopy Core processed samples for electron microscopic analyses, and Mrs. Ann Chavis in Experimental Pathology Lab evaluated pulmonary histopathology. Drs. Stavros Garantziotis and Hideki Nakano at the NIEHS provided excellent critical review of the manuscript.

REFERENCES

1. Kutta H, Wilier A, Steven P, Brauer L, Tsokos M, Paulsen F. Distribution of mucins and antimicrobial substances lysozyme and lactoferrin in the laryngeal subglottic region. J Anat. 2008;213(4):473–481. [PubMed: 18657260]
2. Fahy JV, Dickey BF. Airway mucus function and dysfunction. New Eng J Med. 2010;363(23):2233–2247. [PubMed: 21121836]
3. Okuda K, Chen G, Subramani DB, et al. Localization of Secretory Mucins MUC5AC and MUC5B in Normal/Healthy Human Airways. Am J Respir Crit Care Med. 2019;199(6):715–727. [PubMed: 30352166]
4. Curran DR, Cohn L. Advances in mucous cell metaplasia: a plug for mucus as a therapeutic focus in chronic airway disease. Am J Respir Cell Mol Biol 2010;42(3):268–275. [PubMed: 19520914]
5. Widdicombe JH, Wine JJ. Airway Gland Structure and Function. Physiol Rev. 2015;95(4):1241–1319. [PubMed: 26336032]
6. Dijkstra AE, Boezen HM, van den Berge M, et al. Dissecting the genetics of chronic mucus hypersecretion in smokers with and without COPD. Eur Respir J. 2015;45(1):60–75. [PubMed: 25234806]
7. Stoltz DA, Meyerholz DK, Welsh MJ. Origins of cystic fibrosis lung disease. New Eng J Med 2015;372(4):351–362. [PubMed: 25607428]
8. Ma J, Rubin BK, Voynow JA. Mucins, Mucus, and Goblet Cells. Chest. 2018;154(1):169–176. [PubMed: 29170036]
9. Corfield AP. Mucins: a biologically relevant glycan barrier in mucosal protection. Biochim Biophys Acta. 2015;1850(1):236–252. [PubMed: 24821013]
10. Norman PJ, Norberg SJ, Guethlein LA, et al. Sequences of 95 human MHC haplotypes reveal extreme coding variation in genes other than highly polymorphic HLA class I and II. Genome Res. 2017;27(5):813–823. [PubMed: 28360230]
11. Turner J, Jones CE. Regulation of mucin expression in respiratory diseases. Biochem Soc Trans. 2009;37(Pt 4):877–881. [PubMed: 19614611]
12. Groneberg DA, Eynott PR, Oates T, et al. Expression of MUC5AC and MUC5B mucins in normal and cystic fibrosis lung. Respir Med. 2002;96(2):81–86. [PubMed: 11860173]

13. Inoue D, Kubo H, Watanabe M, et al. Submucosal gland cells in human lower airways produce MUC5AC protein. Respirology. 2008;13(2):285–287. [PubMed: 18339030]
14. Evans CM, Williams OW, Tuvim MJ, et al. Mucin is produced by clara cells in the proximal airways of antigen-challenged mice. Am J Respir Cell Mol Biol. 2004;31(4):382–394. [PubMed: 15191915]
15. Roy MG, Livraghi-Butrico A, Fletcher AA, et al. Muc5b is required for airway defence. Nature. 2014;505(7483):412–416. [PubMed: 24317696]
16. Ehre C, Worthington EN, Liesman RM, et al. Overexpressing mouse model demonstrates the protective role of Muc5ac in the lungs. Proc Natl Acad Sci U.S.A 2012;109(41):16528–16533. [PubMed: 23012413]
17. Chen G, Korfhagen TR, Xu Y, et al. SPDEF is required for mouse pulmonary goblet cell differentiation and regulates a network of genes associated with mucus production. J Clin Invest. 2009;119(10):2914–2924. [PubMed: 19759516]
18. Jiao J, Zhang T, Zhang Y, et al. Epidermal growth factor upregulates expression of MUC5AC via TMEM16A, in chronic rhinosinusitis with nasal polyps. Allergy Asthma Clin Immunol. 2020;16:40. [PubMed: 32514271]
19. Wan H, Kaestner KH, Ang SL, et al. Foxa2 regulates alveolarization and goblet cell hyperplasia. Development. 2004;131(4):953–964. [PubMed: 14757645]
20. Gray T, Nettesheim P, Loftin C, et al. Interleukin-1beta-induced mucin production in human airway epithelium is mediated by cyclooxygenase-2, prostaglandin E2 receptors, and cyclic AMP-protein kinase A signaling. Mol Pharmacol. 2004;66(2):337–346. [PubMed: 15266025]
21. Nordman H, Davies JR, Lindell G, de Bolos C, Real F, Carlstedt I. Gastric MUC5AC and MUC6 are large oligomeric mucins that differ in size, glycosylation and tissue distribution. The Biochemical journal. 2002;364(Pt 1):191–200. [PubMed: 11988092]
22. Matull WR, Andreola F, Loh A, et al. MUC4 and MUC5AC are highly specific tumour-associated mucins in biliary tract cancer. British journal of cancer. 2008;98(10):1675–1681. [PubMed: 18475301]
23. Harkema JR, Carey SA, Wagner JG. The nose revisited: a brief review of the comparative structure, function, and toxicologic pathology of the nasal epithelium. Toxicol Pathol. 2006;34(3):252–269. [PubMed: 16698724]
24. Buisine MP, Devisme L, Copin MC, et al. Developmental mucin gene expression in the human respiratory tract. Am J Respir Cell Mol Biol. 1999;20(2):209–218. [PubMed: 9922211]
25. Chen Y, Zhao YH, Kalaslavadi TB, et al. Genome-wide search and identification of a novel gel-forming mucin MUC19/Muc19 in glandular tissues. Am J Respir Cell Mol Biol. 2004;30(2):155–165. [PubMed: 12882755]
26. Whimster WF. Tracheobronchial submucous gland profiles in smokers and non-smokers. Appl Pathol. 1988;6(4):241–246. [PubMed: 3179066]
27. Evans CM, Raclawska DS, Ttofali F, et al. The polymeric mucin Muc5ac is required for allergic airway hyperreactivity. Nat Commun. 2015;6:6281. [PubMed: 25687754]
28. Koeppen M, McNamee EN, Brodsky KS, et al. Detrimental role of the airway mucin Muc5ac during ventilator-induced lung injury. Mucosal Immunol. 2013;6(4):762–775. [PubMed: 23187315]
29. Cho HY, Gladwell W, Yamamoto M, Kleeberger SR. Exacerbated airway toxicity of environmental oxidant ozone in mice deficient in Nrf2. Oxid Med Cell Longev. 2013;2013:254069. [PubMed: 23766849]
30. Cho HY, Jedlicka AE, Reddy SP, et al. Role of NRF2 in protection against hyperoxic lung injury in mice. Am J Respir Cell Mol Biol. 2002;26(2):175–182. [PubMed: 11804867]
31. Cho HY, Morgan DL, Bauer AK, Kleeberger SR. Signal transduction pathways of tumor necrosis factor--mediated lung injury induced by ozone in mice. Am J Respir Crit Care Med. 2007;175(8):829–839. [PubMed: 17255564]
32. Farraj AK, Harkema JR, Kaminski NE. Allergic rhinitis induced by intranasal sensitization and challenge with trimellitic anhydride but not with dinitrochlorobenzene or oxazolone in A/J mice. Tox Sci. 2004;79(2):315–325.

33. Cho HY, Hotchkiss JA, Harkema JR. Inflammatory and epithelial responses during the development of ozone-induced mucous cell metaplasia in the nasal epithelium of rats. Tox Sci. 1999;51(1):135–145.
34. Hotchkiss JA, Harkema JR, Henderson RF. Effect of cumulative ozone exposure on ozone-induced nasal epithelial hyperplasia and secretory metaplasia in rats. Exp Lung Res. 1991;17(3):589–600. [PubMed: 1860456]
35. Harkema JR, Plopper CG, Hyde DM, St George JA, Dungworth DL. Effects of an ambient level of ozone on primate nasal epithelial mucosubstances. Quantitative histochemistry. Am J Pathol. 1987;127(1):90–96. [PubMed: 3565540]
36. Floyd AM, Zhou X, Evans C, et al. Mucin deficiency causes functional and structural changes of the ocular surface. PloS One. 2012;7(12):e50704. [PubMed: 23272068]
37. Rogers DF. Airway mucus hypersecretion in asthma: an undervalued pathology? Curr Opin Pharmacol. 2004;4(3):241–250. [PubMed: 15140415]
38. Miyahara N, Shoda J, Ishige K, et al. MUC4 interacts with ErbB2 in human gallbladder carcinoma: potential pathobiological implications. Eur J Cancer. 2008;44(7):1048–1056. [PubMed: 18397823]
39. Chakraborty S, Jain M, Sasson AR, Batra SK. MUC4 as a diagnostic marker in cancer. Expert Opin Med Diagn. 2008;2(8):891–910. [PubMed: 23495864]
40. Wang IJ, Yu CJ, Hu FR. Alteration of ocular surface mucins in MUC5AC-DTA transgenic mice. Mol Vis. 2009;15:108–119. [PubMed: 19158956]
41. Dogru M, Okada N, Asano-Kato N, et al. Alterations of the ocular surface epithelial mucins 1, 2, 4 and the tear functions in patients with atopic keratoconjunctivitis. Clin Exp Allergy. 2006;36(12):1556–1565. [PubMed: 17177679]
42. van de Graaf EA, Out TA, Kobesen A, Jansen HM. Lactoferrin and secretory IgA in the bronchoalveolar lavage fluid from patients with a stable asthma. Lung. 1991;169(5):275–283. [PubMed: 1745058]
43. Young HW, Williams OW, Chandra D, et al. Central role of Muc5ac expression in mucous metaplasia and its regulation by conserved 5′ elements. Am J Respir Cell Mol Biol. 2007;37(3):273–290. [PubMed: 17463395]
44. Bonser LR, Zlock L, Finkbeiner W, Erle DJ. Epithelial tethering of MUC5AC-rich mucus impairs mucociliary transport in asthma. J Clin Invest. 2016;126(6):2367–2371. [PubMed: 27183390]
45. Hallstrand TS, Debley JS, Farin FM, Henderson WR, Jr. Role of MUC5AC in the pathogenesis of exercise-induced bronchoconstriction. J Allergy Clin Immunol. 2007;119(5):1092–1098. [PubMed: 17321575]
46. Henderson AG, Ehre C, Button B, et al. Cystic fibrosis airway secretions exhibit mucin hyperconcentration and increased osmotic pressure. J Clin Invest. 2014;124(7):3047–3060. [PubMed: 24892808]
47. Ha EV, Rogers DF. Novel Therapies to Inhibit Mucus Synthesis and Secretion in Airway Hypersecretory Diseases. Pharmacology. 2016;97(1–2):84–100. [PubMed: 26674354]
48. Bonser LR, Erle DJ. Airway Mucus and Asthma: The Role of MUC5AC and MUC5B. J Clin Med 2017;6(12).
49. Johnson L, Shah I, Loh AX, et al. MUC5AC and inflammatory mediators associated with respiratory outcomes in the British 1946 birth cohort. Respirology. 2013;18(6):1003–1010. [PubMed: 23551418]
50. Guo X, Pace RG, Stonebraker JR, et al. Mucin variable number tandem repeat polymorphisms and severity of cystic fibrosis lung disease: significant association with MUC5AC. PloS One. 2011;6(10):e25452. [PubMed: 21998660]
51. Amini SE, Gouyer V, Portal C, Gottrand F, Desseyn JL. Muc5b is mainly expressed and sialylated in the nasal olfactory epithelium whereas Muc5ac is exclusively expressed and fucosylated in the nasal respiratory epithelium. Histochem Cell Biol. 2019.
52. Evans CM, Fingerlin TE, Schwarz MI, et al. Idiopathic Pulmonary Fibrosis: A Genetic Disease That Involves Mucociliary Dysfunction of the Peripheral Airways. Physiol Rev. 2016;96(4):1567–1591. [PubMed: 27630174]

53. Gondran C, Dubois MP, Fort S, Cosnier S, Szunerits S. Detection of carbohydrate-binding proteins by oligosaccharide-modified polypyrrole interfaces using electrochemical surface plasmon resonance. Analyst. 2008;133(2):206–212. [PubMed: 18227943]
54. Petrou G, Crouzier T. Mucins as multifunctional building blocks of biomaterials. Biomater Sci. 2018;6(9):2282–2297. [PubMed: 30047553]
55. Vareille M, Kieninger E, Edwards MR, Regamey N. The airway epithelium: soldier in the fight against respiratory viruses. Clin Microbiol Rev. 2011;24(1):210–229. [PubMed: 21233513]
56. Hackett NR, Shaykhiev R, Walters MS, et al. The human airway epithelial basal cell transcriptome. PloS One. 2011;6(5):e18378. [PubMed: 21572528]
57. Tyner JW, Kim EY, Ide K, et al. Blocking airway mucous cell metaplasia by inhibiting EGFR antiapoptosis and IL-13 transdifferentiation signals. J Clin Invest. 2006;116(2):309–321. [PubMed: 16453019]
58. Danahay H, Pessotti AD, Coote J, et al. Notch2 is required for inflammatory cytokine-driven goblet cell metaplasia in the lung. Cell Rep. 2015;10(2):239–252. [PubMed: 25558064]
59. Cohn L Mucus in chronic airway diseases: sorting out the sticky details. J CLin Invest. 2006;116(2):306–308. [PubMed: 16453018]
60. Ostedgaard LS, Moninger TO, McMenimen JD, et al. Gel-forming mucins form distinct morphologic structures in airways. Proc Natl Acad Sci U.S.A 2017;114(26):6842–6847. [PubMed: 28607090]
61. Hayashi T, Ishii A, Nakai S, Hasegawa K. Ultrastructure of goblet-cell metaplasia from Clara cell in the allergic asthmatic airway inflammation in a mouse model of asthma in vivo. Virchows Arch. 2004;444(1):66–73. [PubMed: 14648220]
62. Reader JR, Tepper JS, Schelegle ES, et al. Pathogenesis of mucous cell metaplasia in a murine asthma model. Am J Pathol. 2003;162(6):2069–2078. [PubMed: 12759261]
63. Smallcombe CC, Linfield DT, Harford TJ, et al. Disruption of the airway epithelial barrier in a murine model of respiratory syncytial virus infection. Am J Physiol Lung Cell Mol Physiol. 2019;316(2):L358–L368. [PubMed: 30489157]
64. Thannickal VJ, Toews GB, White ES, Lynch JP 3rd, Martinez FJ. Mechanisms of pulmonary fibrosis. Annu Rev Med. 2004;55:395–417. [PubMed: 14746528]
65. Michaudel C, Mackowiak C, Maillet I, et al. Ozone exposure induces respiratory barrier biphasic injury and inflammation controlled by IL-33. J Allergy Clin Immunol. 2018;142(3):942–958. [PubMed: 29331644]
66. Post S, Heijink IH, Hesse L, et al. Characterization of a lung epithelium specific E-cadherin knock-out model: Implications for obstructive lung pathology. Sci Rep. 2018;8(1):13275. [PubMed: 30185803]
67. Muthupalani S, Ge Z, Joy J, et al. Muc5ac null mice are predisposed to spontaneous gastric antro-pyloric hyperplasia and adenomas coupled with attenuated H. pylori-induced corpus mucous metaplasia. Lab Invest. 2019.
68. Bauer AK, Umer M, Richardson VL, et al. Requirement for MUC5AC in KRAS-dependent lung carcinogenesis. JCI Insight. 2018;3(15).

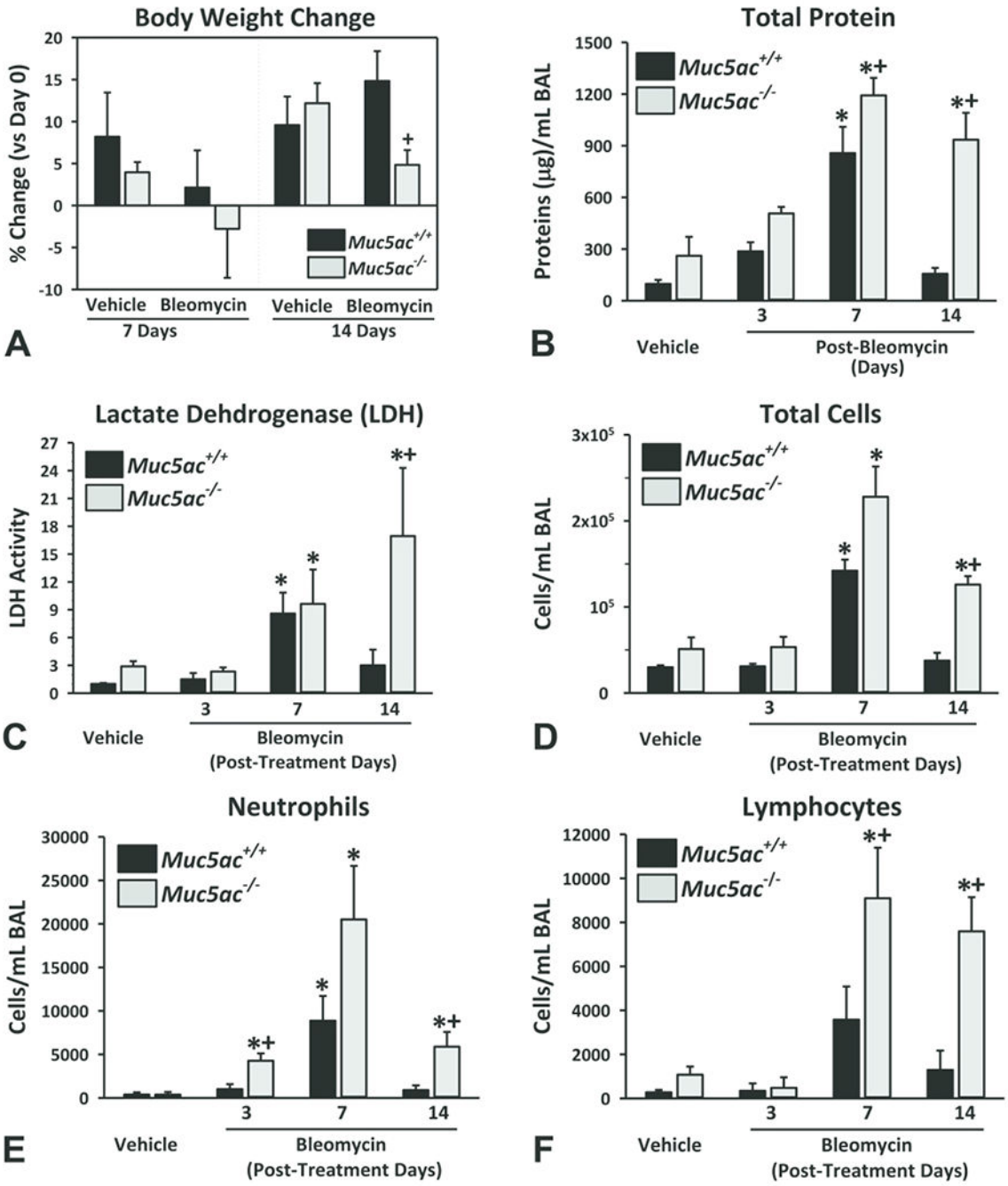

Figure 1. Enhanced bleomycin-induced lung injury in mucin-5AC-deficient (*Muc5ac*$^{-/-}$) mice.

Body weight change (A) and bronchoalveolar lavage (BAL) analysis for protein concentration (B) and lactate dehydrogenase concentration (C) as well as the number of total cells (D), neutrophils (E) and lymphocytes (F) were determined in wild-type (*Muc5ac*$^{+/+}$) and *Muc5ac*$^{-/-}$ mice after vehicle or bleomycin instillation. Data presented as mean ± SEM (n = 3-7 mice/group for body weight, 6-8 mice/group for vehicle-BAL, n = 3/group for 3-day bleomycin-BAL, n = 5-7 for 7- and 14-day bleomycin-BAL). Graph symbols; *$P < 0.05$

vs. genotype-matched vehicle control mice, †$P < 0.05$ vs. exposure-matched *Muc5ac*$^{+/+}$ mice.

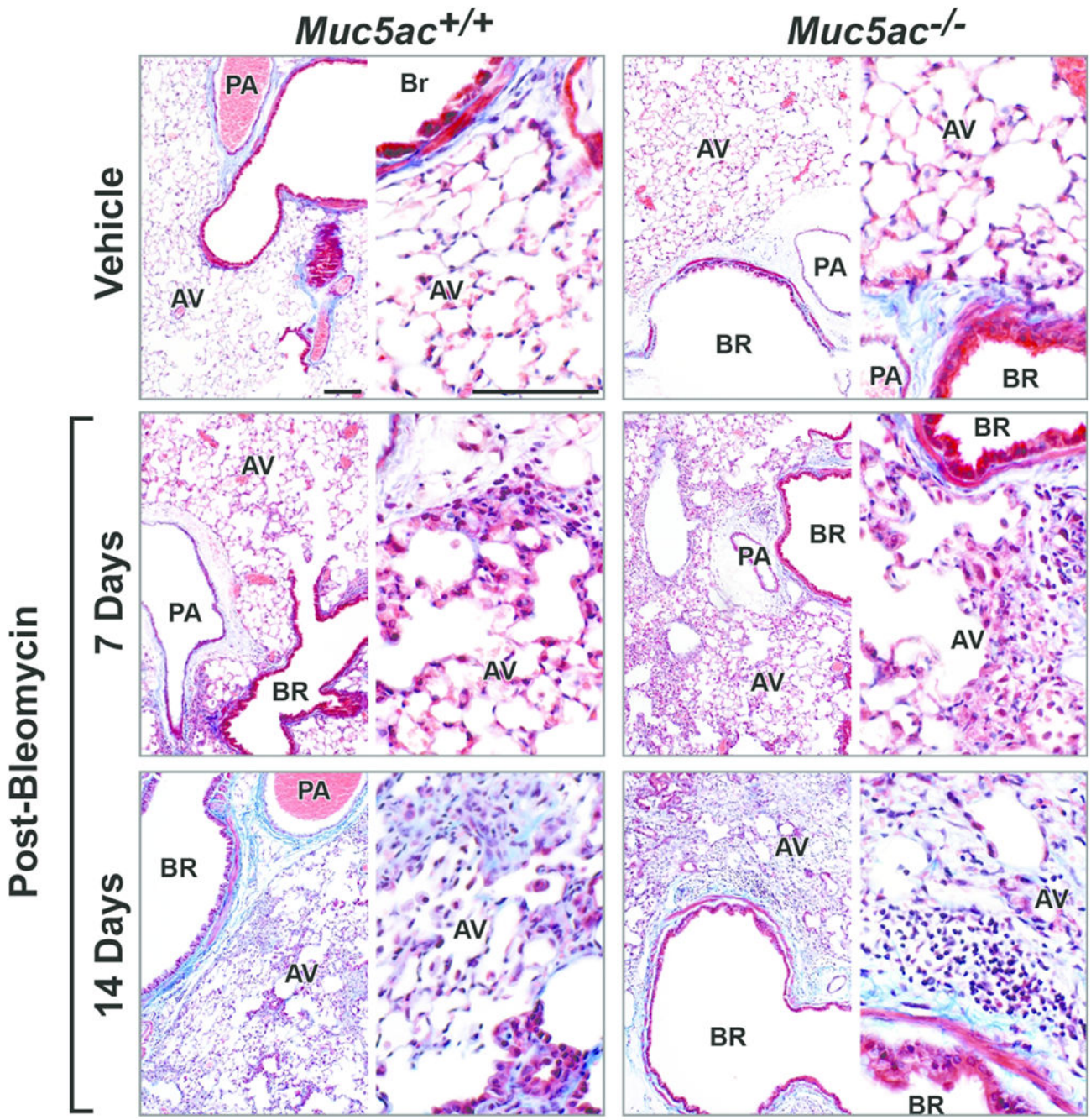

Figure 2. Augmented bleomycin-induced pulmonary histopathology in mucin-5AC-deficient (*Muc5ac*$^{-/-}$) mice.

Masson's trichrome staining exhibits differential progress and severity of pulmonary fibrosis and collagen accumulation between wild-type (*Muc5ac*$^{+/+}$) and *Muc5ac*$^{-/-}$ mice at 7- and 14-days post-bleomycin or at 14-days post vehicle. Representative light photomicrographs of lung sections (n=6-7/group) were presented. Bar = 100 μm. AV = alveoli. BR = bronchi or bronchiole. PA = pulmonary artery.

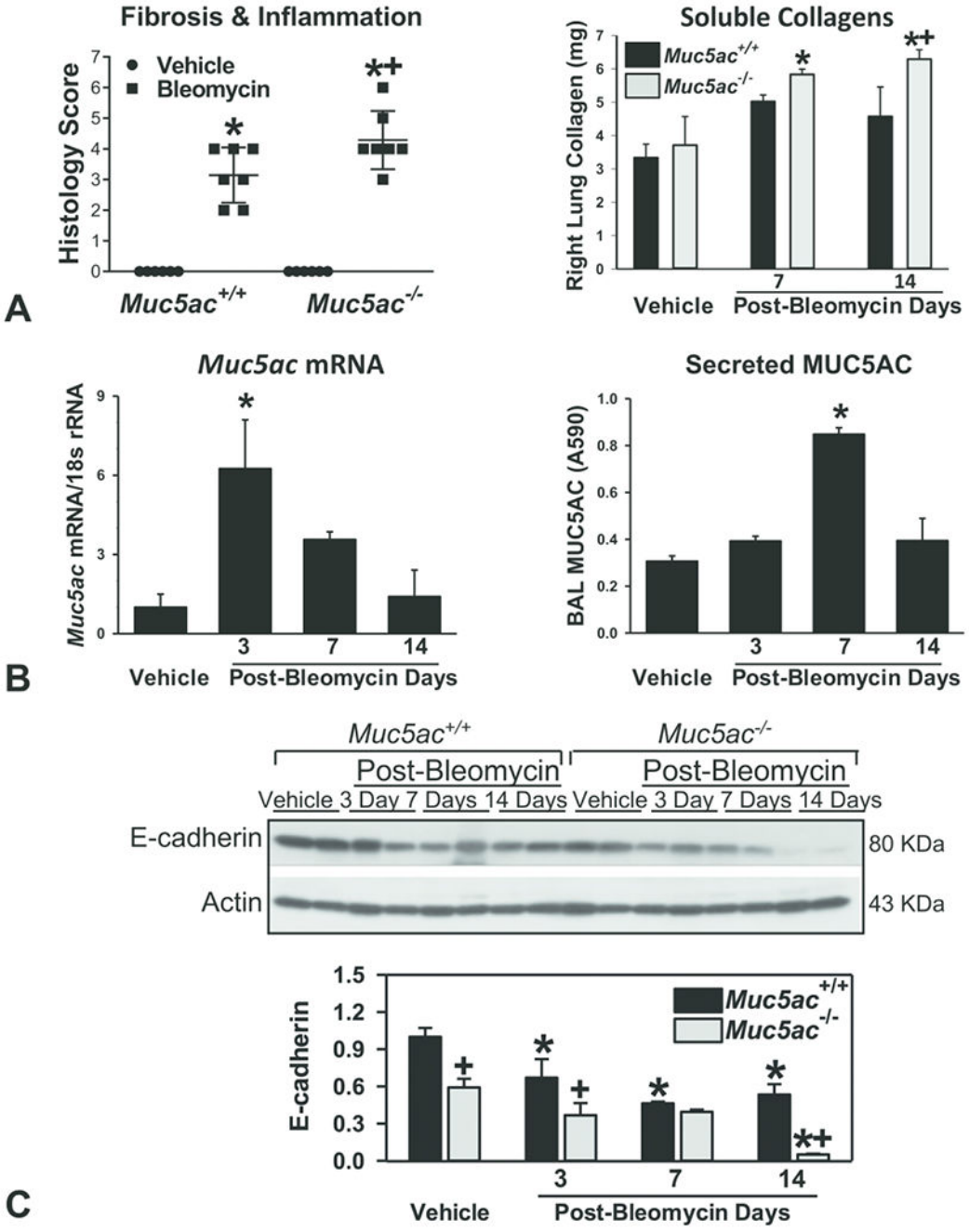

Figure 3. Bleomycin-induced changes in fibrotic lung injury, mucin-5AC (MUC5AC), and epithelial barrier expression in mucin-5AC-sufficient (*Muc5ac*$^{+/+}$) and -deficient (*Muc5ac*$^{-/-}$) mice.

(A) Severity of histopathologic lung inflammation and fibrosis at 14 days post-bleomycin was scored by microscopic evaluation of H&E and Masson's trichrome-stained slides (n = 6-7/group). Total soluble collagen contents were determined in whole right lung lysates using a colorimetric Sirius Red dye-collagen binding assay. Mean ± SEM presented (n = 4/group). (B) Pulmonary *Muc5ac* mRNA expression was determined by qRT-PCR using a mouse specific *Muc5ac* primer set in *Muc5ac*$^{+/+}$ mice (n = 3/group). Secreted Muc5ac level

was determined in the aliquots of bronchoalveolar lavage supernatants from *Muc5ac*$^{+/+}$ mice using a sandwich enzyme-linked immunosorbent assay (n = 3-4/group). Mean ± SEM presented. (C) Protein level of E-cadherin in aliquots of lung homogenates was determined by Western blot analysis using actin as an internal control (n = 2 pooled samples/group). Representative digitized images from duplicate assays are presented. Intensity of blot images were quantified by densitometry (n = 2/group, Mean ± SEM presented). Graph symbols; *$P < 0.05$ vs. genotype-matched vehicle control mice. †$P < 0.05$ vs. exposure-matched *Muc5ac*$^{+/+}$ mice.

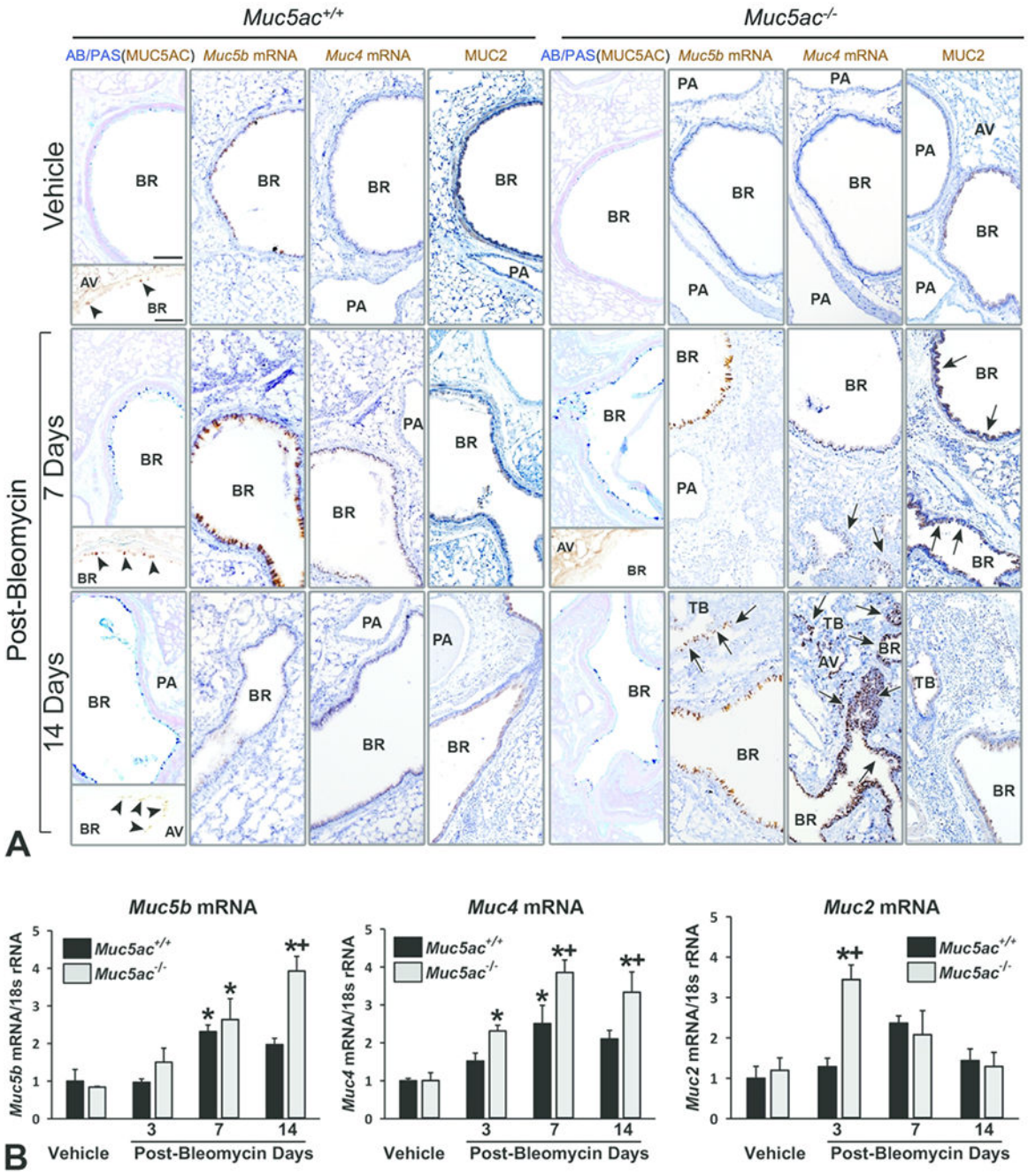

Figure 4. Bleomycin-induced compensatory mucin overexpression in mucin-5AC-deficient (*Muc5ac*$^{-/-}$) mouse lungs.

(A) Mucus in conducting airways was visualized by AB/PAS-stained proximal aspect of left lung sections from vehicle (14 days) and bleomycin (7 and 14 days)-treated mice. Expression and localization of single mucin was determined by immunohistochemical staining (IHC) using specific antibodies for MUC5AC (insets in AB/PAS) and MUC2 or *in situ* hybridization (ISH) using specific probes for *Muc5b* and *Muc4* on the serial cuts of the same tissue blocks. Arrow heads indicate Muc5ac proteins localized in bronchial epithelium of *Muc5ac*$^{+/+}$ mice. Arrows indicate more markedly increased *Muc4* and *Muc5b* message or

MUC2 protein in *Muc5ac*$^{-/-}$ mice compared to those in *Muc5ac*$^{+/+}$ mice. Representative light micrographs presented. Bars = 100 μm. AV = alveoli. BR = bronchi or bronchiole. PA = pulmonary artery. TB = terminal bronchiole. (B) Pulmonary *Muc5b, Muc4*, and *Muc2* mRNA expressions were determined by qRT-PCR using mouse specific primer sets (n = 3/group). Mean ± SEM presented. Graph symbols; *$P < 0.05$ vs. genotype-matched vehicle control mice. †$P < 0.05$ vs. exposure-matched *Muc5ac*$^{+/+}$ mice.

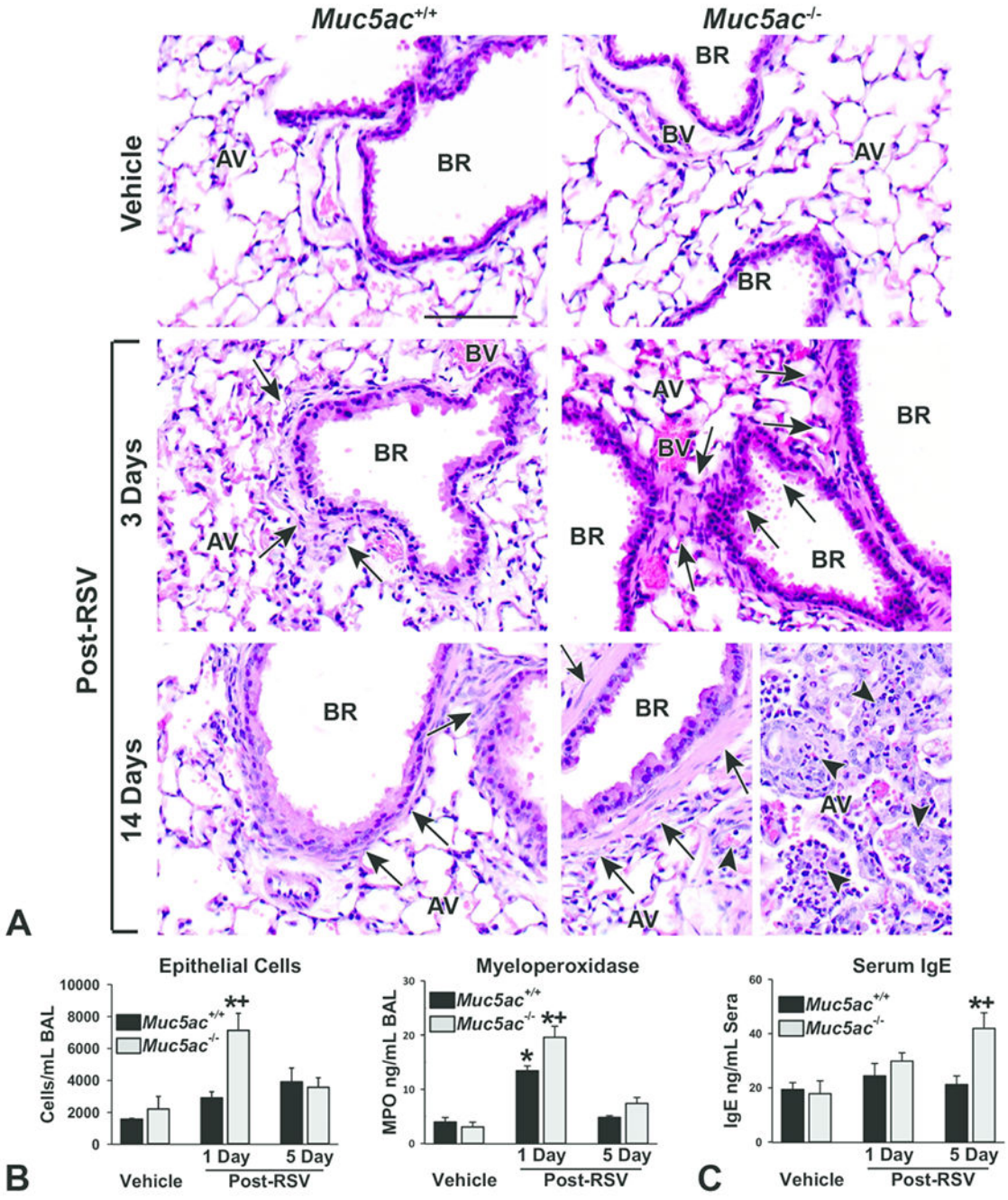

Figure 5. Exacerbated respiratory syncytial virus (RSV)-induced pulmonary injury and airway narrowing in mucin-5AC-deficient (*Muc5ac*$^{-/-}$) mice.

(A) Differential severe bronchial/bronchiolar hyperplasia and hypertrophy and smooth muscle thickening in *Muc5ac*$^{-/-}$ mice than in *Muc5ac*$^{+/+}$ mice demonstrated by H&E staining of proximal aspect of left lung after 3-5 days post-RSV infection or 3 days post vehicle. Large syncytia (multinucleated cells) formation and lymphocytic inflammation in alveoli were detected more markedly in *Muc5ac*$^{-/-}$ mice at 5 days post-RSV. Representative light photomicrographs presented (n = 5-8/group). Arrows indicate perivascular-peribronchiolar edema and smooth muscle hyperplasia. Arrow heads indicate syncytia. AV =

alveoli. BR = bronchi or bronchiole. Bar = 100 μm. (B) Significantly higher number of epithelial cells and concentration of neutrophil myeloperoxidase (MPO) in bronchoalveolar lavage (BAL) fluids from *Muc5ac*$^{-/-}$ mice compared to those in *Muc5ac*$^{+/+}$ after 1-day post-RSV infection. Mean ± SEM (n = 4-8/group for epithelial cells, n = 4-5/group for MPO) presented. (C) Immunoglobulin E (IgE) level determined in aliquots of serum (1 μL) using a colorimetric enzyme-linked immunosorbent assay kit. Mean ± SEM (n = 3/group) presented. Graph symbols; *$P < 0.05$ vs. genotype-matched vehicle control mice. †$P < 0.05$ vs. exposure-matched *Muc5ac*$^{+/+}$ mice.

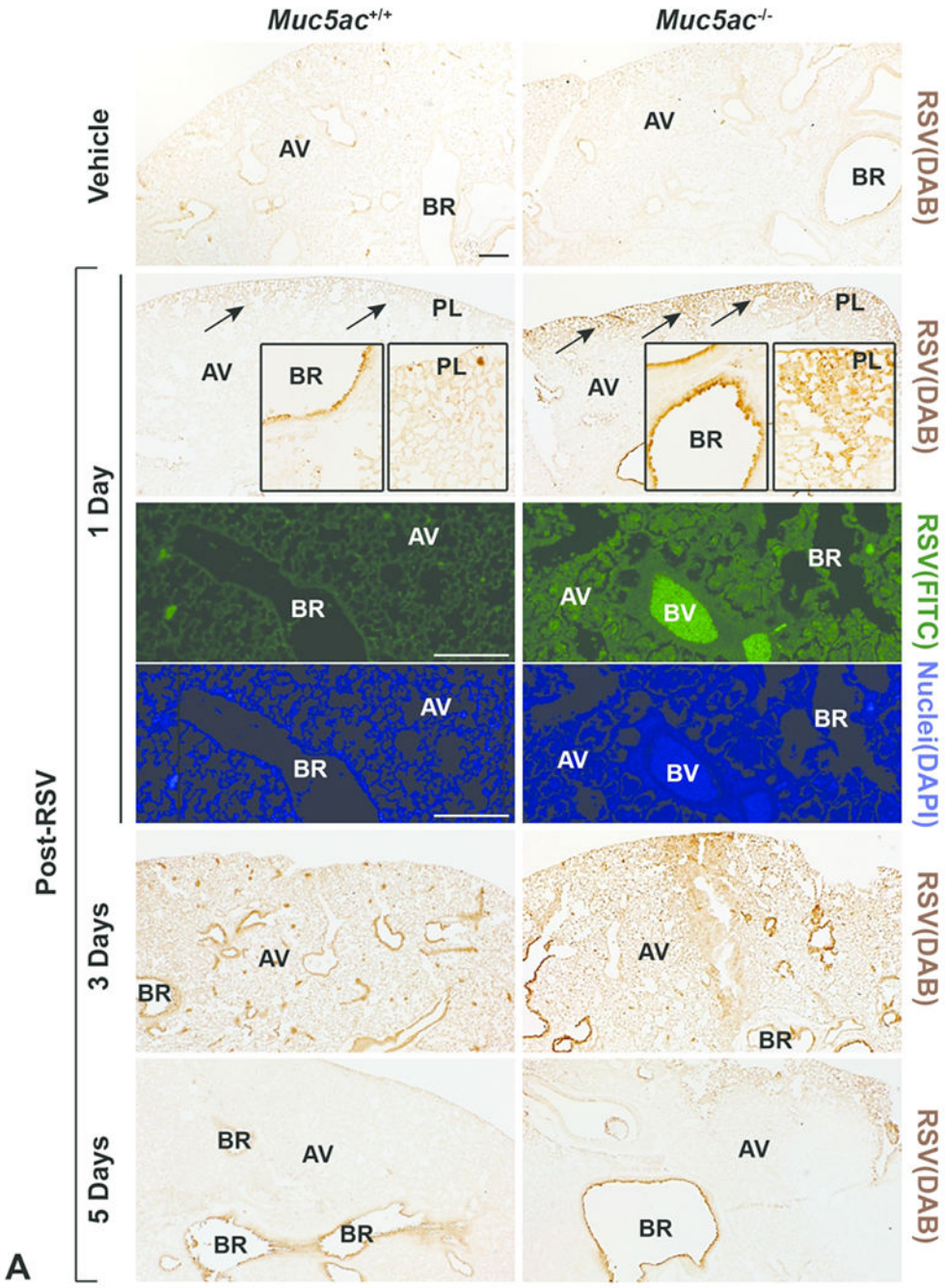

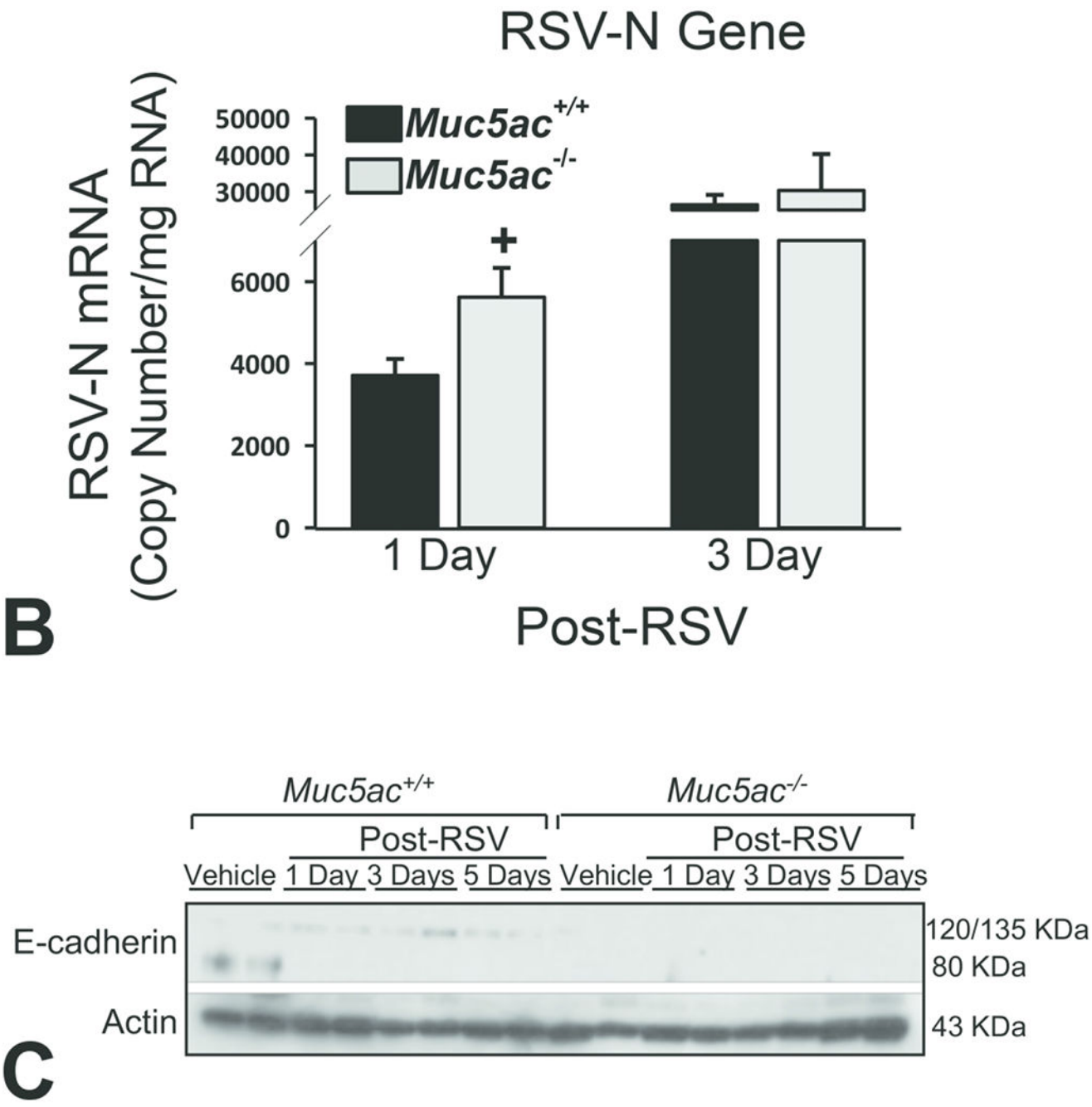

Figure 6. Differential respiratory syncytial virus (RSV) load and epithelial barrier expression in mucin-5AC-sufficient (*Muc5ac*$^{+/+}$) and -deficient (*Muc5ac*$^{-/-}$) mouse lungs.

(A) RSV localization in lung sections detected by immunohistochemical (DAB) and immunofluorescent (FITC) methods using an anti-RSV antibody. Arrows indicate virus enrichment in pleurae (pleuritis) at 1-day post-RSV infection detected by DAB. Confocal images display more diffused RSV visualized with fluorescence (green, top) in *Muc5ac*$^{-/-}$ mouse lung than in *Muc5ac*$^{+/+}$ lung. Nuclei were stained with DAPI (blue, bottom). Bars = 200 μm. AV = alveoli. BR = bronchi or bronchiole. PL = pleurae (pleural cavity). BV = blood vessel. Representative light photomicrographs presented (n = 5-8/group). (B) RSV

infectivity was determined by quantification of viral nucleoprotein (N) gene expression using a digitized droplet PCR (ddPCR) method. Mean ± SEM (n = 3/group) presented. (C) Protein level of E-cadherin in aliquots of lung homogenates was determined by Western blot analysis using actin as an internal control (n = 2 pooled samples/group). Representative digitized images from duplicate assays are presented. Graph symbols; $*P < 0.05$ vs. genotype-matched vehicle control mice. $\dagger P < 0.05$ vs. exposure-matched *Muc5ac*$^{+/+}$ mice.

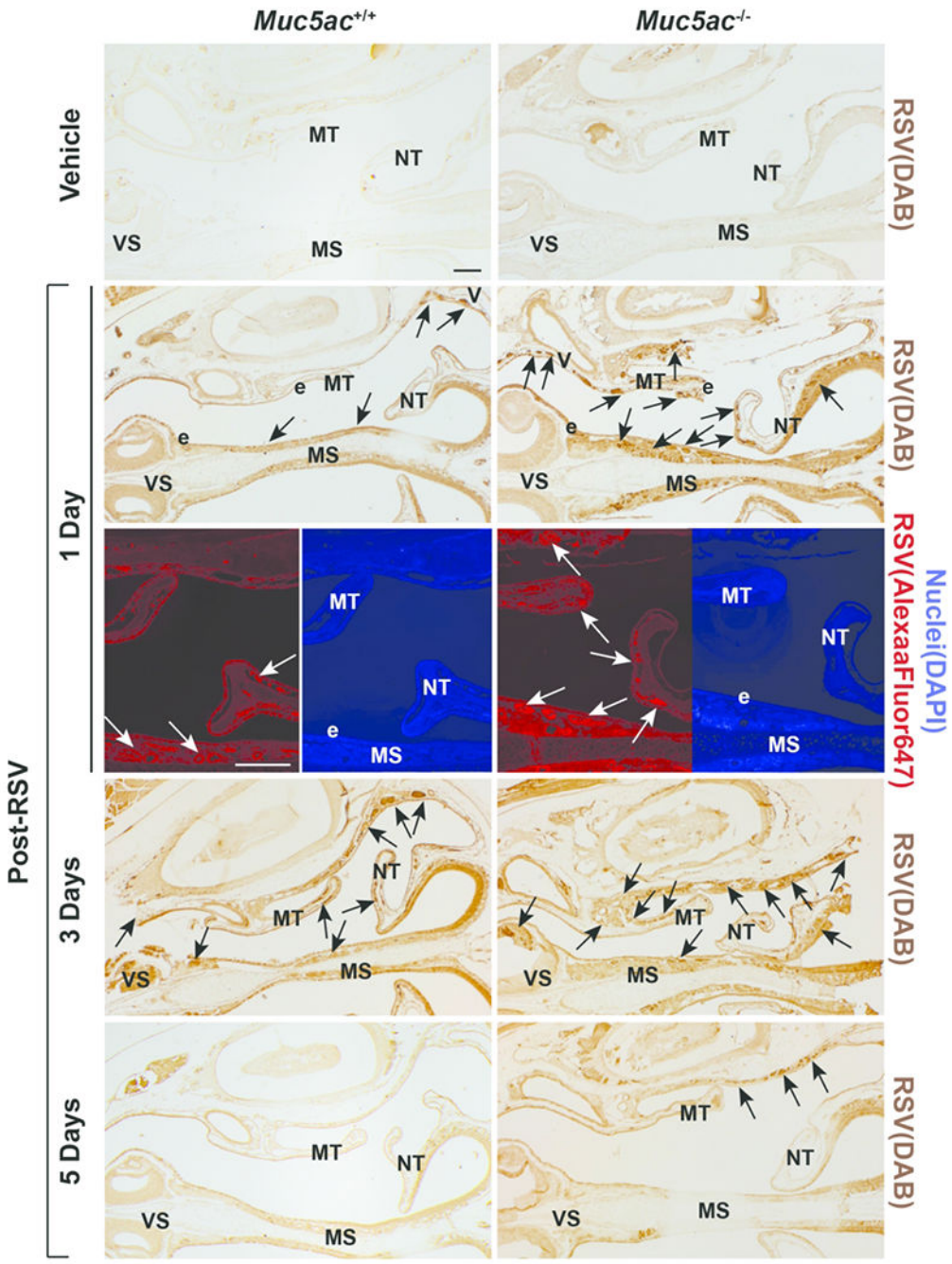

Figure 7. Heightened respiratory syncytial virus (RSV) load in nasal airway of *Muc5ac*-deficient (*Muc5ac*$^{-/-}$) mice.

(A) RSV detected by immunohistochemical (DAB) and immunofluorescent (Alexa Fluor 647) methods in proximal nasal airways of *Muc5ac*$^{+/+}$ and *Muc5ac*$^{-/-}$ mice treated with vehicle (3 days) or RSV (1, 3, 5 days) using an anti-RSV antibody. Confocal images display more diffused virus visualized with fluorescence (left, red) in *Muc5ac*$^{-/-}$ turbinate than in *Muc5ac*$^{+/+}$ turbinate at 1-day post-RSV. Nuclei were stained with DAPI (right, blue). Arrows indicate virus enriched in submucosal glands underneath septum and

maxilloturbinate (MT). e = surface epithelium lining nasal mucosa. VS = ventral septum. NT = nasoturbinate. Bars = 200 μm.

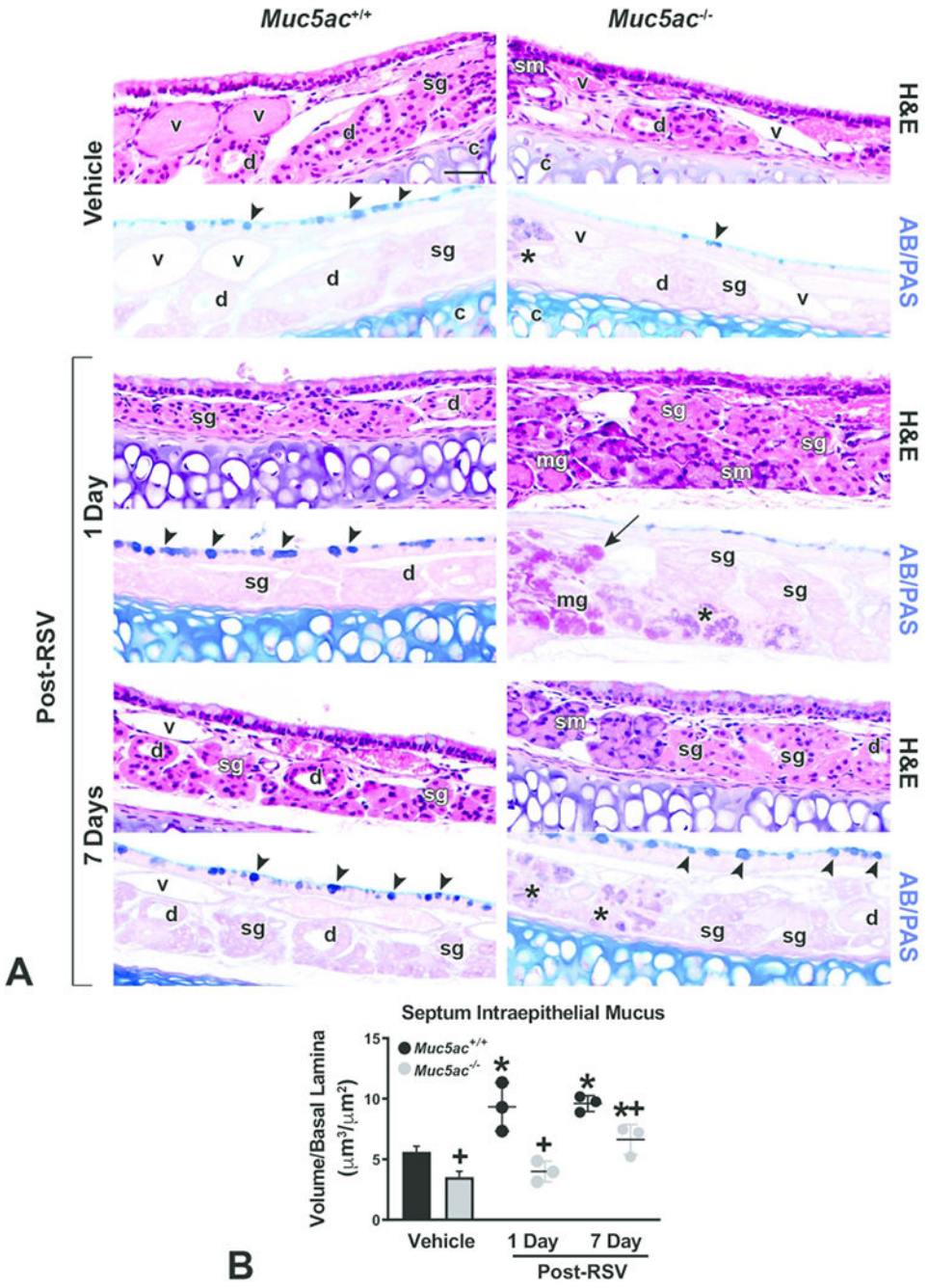

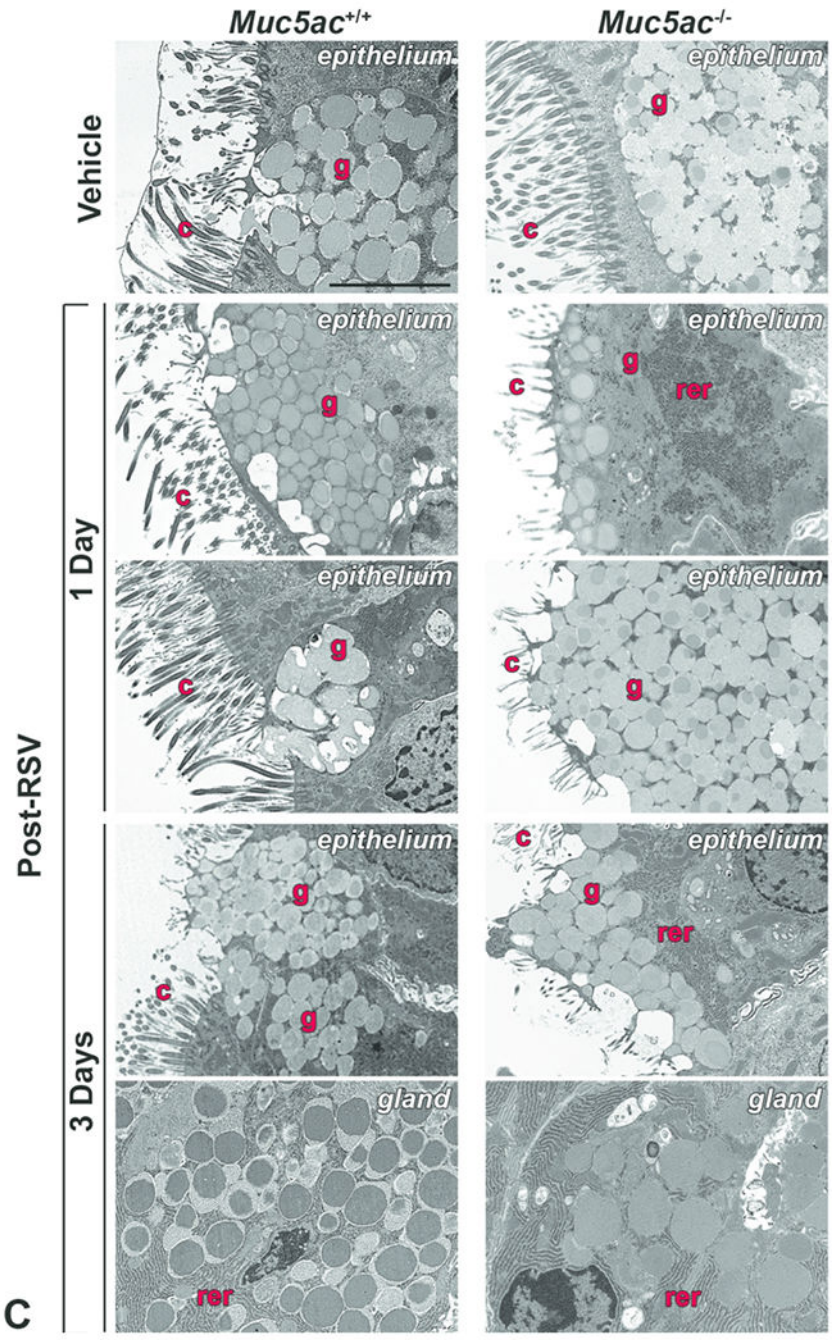

Figure 8. Differential changes of respiratory syncytial virus (RSV)-induced nasal airway mucosubstances in mucin-5AC-sufficient (*Muc5ac*$^{+/+}$) and -deficient (*Muc5ac*$^{-/-}$) mice.

(A) Changes of intraepithelial and submucosal glandular mucosubstances in mid-septum (MS) of vehicle (1 day) and RSV (1 and 7 days)-treated mice. Representative light photomicrographs presented (n = 3-5/group). Arrow heads indicate stored intraepithelial mucus increased early (1 day) in *Muc5ac*$^{+/+}$ mice and later (7 day) in *Muc5ac*$^{+/+}$ and *Muc5ac*$^{-/-}$ vehicle after RSV infection. Arrow indicates PAB-positive mucus in hyperplastic mucosal glands. Asterisks indicate AB/PAS-stained mucus in newly developed glands (potentially submandibular) of *Muc5ac*$^{-/-}$ mouse septum. sg = serous gland. mg = mucous

gland. sm = seromucous (submandibular) gland. d = gland duct. v = blood vessel. c = cartilage. Bar = 50 μm. (B) RSV-induced increase in volume density (Vs) of AB/PAS-stained stored intraepithelial mucus in MS was morphometrically measure by Image J software. Mean ± SEM (n = 3/group) presented. Graph symbols; *$P < 0.05$ vs. genotype-matched vehicle control mice. †$P < 0.05$ vs. exposure-matched *Muc5ac* mice. (C) Transmission electron micrographs of nasal septum from vehicle-treated *Muc5ac*$^{+/+}$ tissue with an intact periciliary layer, ciliated respiratory epithelium, and goblet cell vesicles filled with electron-dense materials (secretory mucins), while goblet cells in vehicle-treated *Muc5ac*$^{-/-}$ septum had relatively reduced granule storage. RSV-infected nasal epithelial cell surface with loss of cilia in both genotypes of mice. Goblet cells in *Muc5ac*$^{+/+}$ mice had more frequent evidence of vacuoles (1 day), viral infection-associated debris trapped in fused granules (1 day), and granule exocytosis (3 day) against RSV indicating active antiviral activity. These goblet cell changes were relatively scarce in RSV-infected *Muc5ac*$^{-/-}$ mice and their secretory granule storage was decreased until 3 days post-RSV. In contrast, subepithelial glands in *Muc5ac*$^{-/-}$ septum contained uniformly-stained granules connected with rich rough endoplasmic reticulum (rer) while subepithelial granules in *Muc5ac*$^{+/+}$ septum had particularly electron-lucent outer rim (3 day). g = surface goblet cell with granules. c = cilia. Bar = 5 μm.

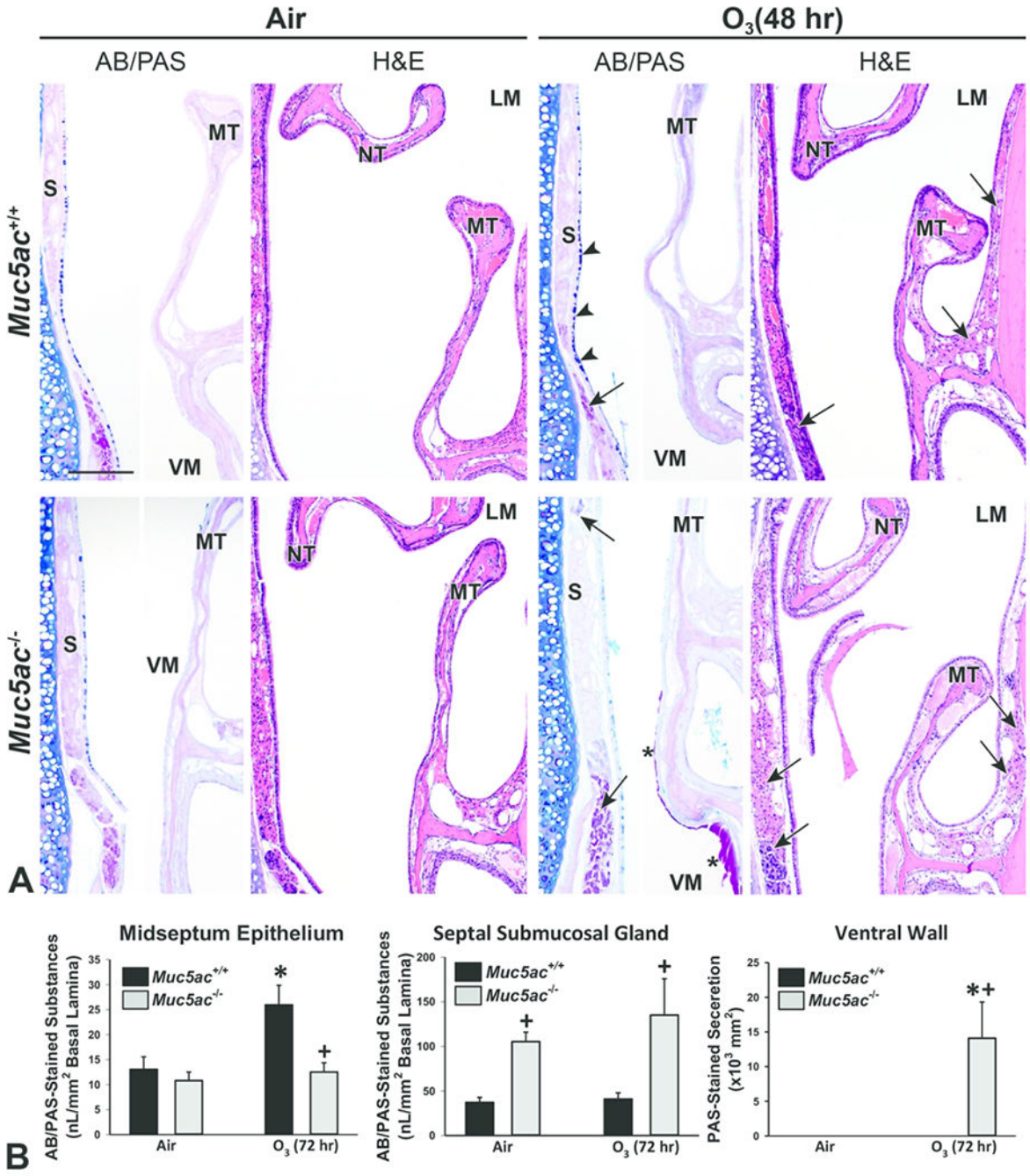

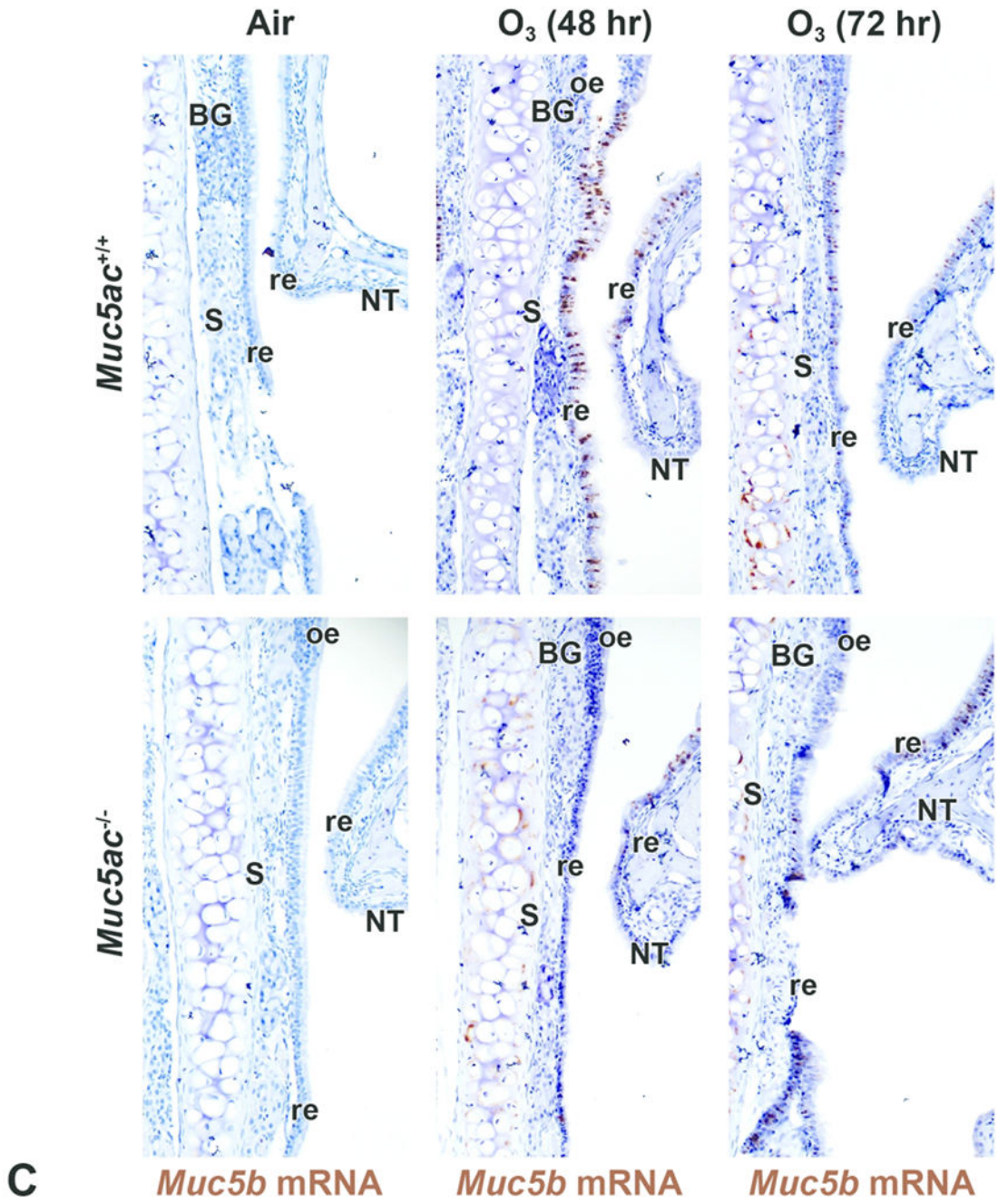

Figure 9. Exacerbation of nasal airway responses to ozone (O_3) exposure in mucin-5AC-deficient (*Muc5ac*$^{-/-}$) mice.

(A) Increase in AB/PAS-stained septal intraepithelial mucosubstances (arrow heads) and PAS-stained septal and lateral wall subepithelial gland mucosubstances (arrows) in *Muc5ac*$^{+/+}$ and *Muc5ac*$^{-/-}$ nasal airways after O_3 exposure (48 hr). PAS-positive mucus-like secretion seen only in O_3-exposed *Muc5ac*$^{-/-}$ terminates was indicated by an asterisk. S = septum. MT = maxilloturbinate. NT = nasoturbinate. LM = lateral meatus. VM = ventral meatus. Bar = 200 μm. (B) Morphometric analyses identified O_3-induced significant increase in AB/PAS-stained intraepithelial mucosubstances in *Muc5ac*$^{+/+}$ turbinate (mid-

septum) and PAS-stained subepithelial gland (mid-ventral septum) and PAS-positive mucus-like secretion (ventral meatus) in *Muc5ac*$^{-/-}$ turbinate. Mean ± SEM (n = 3/air group, n = 4/O_3 group) presented. Graph symbols; *$P < 0.05$ vs. genotype-matched air control mice. †$P < 0.05$ vs. exposure-matched *Muc5ac*$^{+/+}$ mice. (C) Nasal airway *Muc5b* mRNA expression (brown dots) determined by *in situ* hybridization (ISH) was markedly increased by O_3 in respiratory epithelium throughout the septum and nasoturbinate undergoing mucous cell hyperplasia/metaplasia. *Muc5b* mRNA was also detected marginally after O_3 exposure in Bowman's glands. O_3-induced *Muc5b* expression was higher in *Muc5ac*$^{+/+}$ mice than in *Muc5ac*$^{-/-}$ mice, concurrent with AB/PAS-positive mucus increases (peak at 2 days) by O_3 exposure. Bar = 100 μm. S = septum. NT = nasoturbinate. re = respiratory epithelium. oe = olfactory epithelium. BG = bowman's glands.

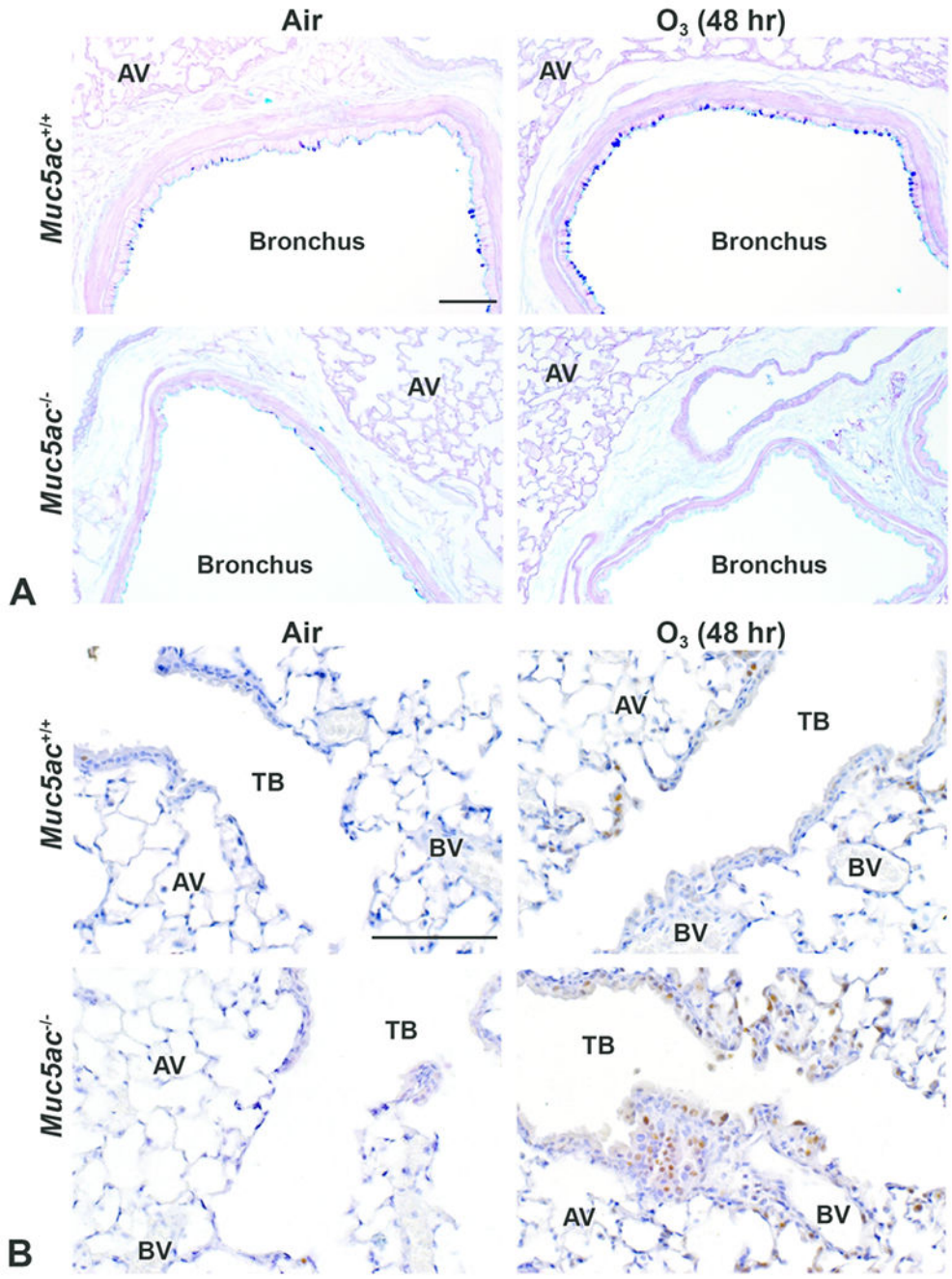

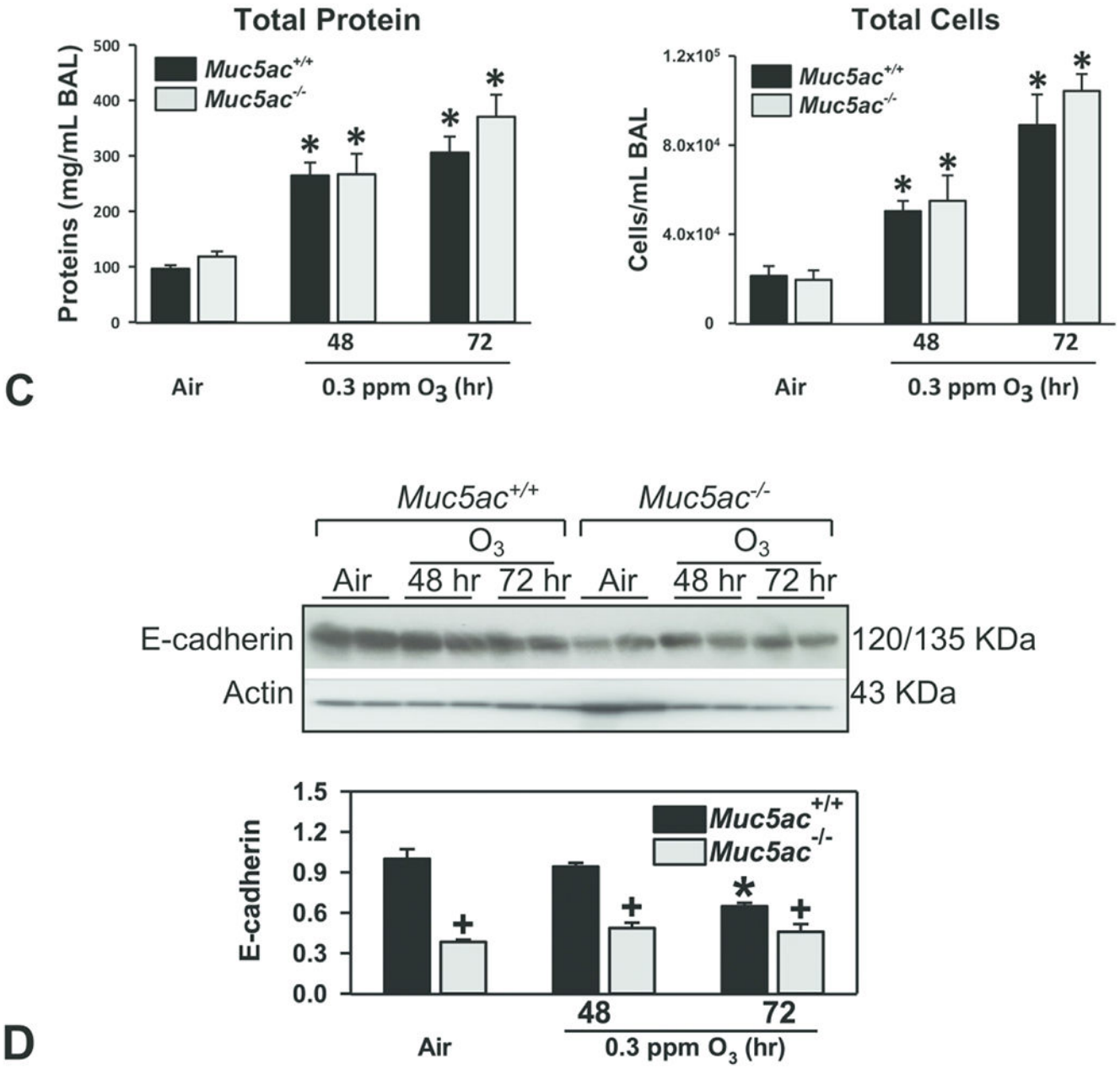

Figure 10. Exacerbation of pulmonary airway responses to ozone (O_3) exposure in mucin-5AC-deficient (*Muc5ac*$^{-/-}$) mice.

(A) AB/PAS staining determined O_3-induced bronchial epithelial mucous cell metaplasia in *Muc5ac*$^{+/+}$ lung (peaked at 48 hr), but not in *Muc5ac*$^{-/-}$ lung. AV = alveoli. Bar = 100 μm. (B) Epithelial cell proliferation in terminal bronchiole of centriacinal region, a marker of pulmonary O_3 sensitivity, was determined by immunohistochemical staining of proliferating cell nuclear antigen (PCNA). Brown dots = PCNA. AV = alveoli. BR=bronchiole. TB = terminal bronchiole. BV = blood vessel. Bar = 100 μm. (C) Bronchoalveolar lavage (BAL) analysis found no significant differences in lung protein concentration and cellular injury between *Muc5ac*$^{+/+}$ and *Muc5ac*$^{-/-}$ mice after sub-acute exposure to 0.3 parts per million O_3

exposure. Data presented as mean ± SEM (n = 4 for air groups, n = 6 for O_3 groups). (D) Protein level of E-cadherin in aliquots of lung homogenates was determined by Western blot analysis using actin as an internal control (n = 2 pooled samples/group). Representative digitized images from duplicate assays are presented. Intensity of blot images was quantified by densitometry (n = 2/group, Mean ± SEM presented). Graph symbols; *$P < 0.05$ vs. genotype-matched air control mice. †$P < 0.05$ vs. exposure-matched *Muc5ac*$^{+/+}$ mice.